Title

Modulation of Frontal Oscillatory Power during Blink Suppression in Children: Effects of Premonitory Urge and Reward.

Journal

Cerebral cortex communications, 1(1)

ISSN

2632-7376

Authors

Miyakoshi, Makoto
Jurgiel, Joseph
Dillon, Andrea
et al.

Publication Date

2020

DOI

10.1093/texcom/tgaa046

Peer reviewed

Running title: EEG study on blink suppression in healthy children

Modulation of frontal oscillatory power during blink suppression in children: Effects of premonitory urge and reward

Makoto Miyakoshi[a*], Joseph Jurgiel[b], Andrea Dillon[b], Susanna Chang[b], John Piacentini[b], Scott Makeig[a], Sandra K. Loo[b]

[a]Swartz Center for Neural Computation, Institute for Neural Computation, University of California San Diego, 9500 Gilman Drive La Jolla CA 92093-0559
[b]Semel Institute for Neuroscience and Human Behavior, University of California, Los Angeles, 760 Westwood Plaza, Los Angeles, CA 90095

*Corresponding author:
Makoto Miyakoshi, Ph.D.
Swartz Center for Neural Computation, Institute for Neural Computation, University of California San Diego
9500 Gilman Drive La Jolla CA 92093-0559 USA
Office Phone: 858-825-7534
Email: mmiyakoshi@ucsd.edu

29 pages
6 figures, 0 tables
200 words for abstract
6294 words for the main text

Conflict of interest: The authors declare no competing financial interests.
Acknowledgements: Funding for the current study was provided by National Institutes of Neurological Disease and Stroke grants 80160 and 97484 (SKL). The Swartz Center for Neural Computation, directed by Scott Makeig, was founded in 2001 by a generous gift from founding donor Dr. Jerome Swartz of The Swartz Foundation (Old Field, New York).

Significance statement

We examined dynamics of electroencephalogram (EEG) during blink suppression and modulations in response to premonitory urge and reward conditions among healthy children. We empirically defined the time course of self-reported urge, which may be useful for designing future neuroimaging studies. EEG correlates of effortful urge suppression were localized in the regions related to body control and sensation. Furthermore, EEG evidence supports the effectiveness of using reward to enhance blink suppression. These findings improve neural model of suppression in the presence of urge and reward in future mechanistic studies of Tourette syndrome, Obsessive-Compulsive Disorder, and Body Focused Repetitive Behaviors.

Abstract

There is a dearth of studies examining the underlying mechanisms of blink suppression and the effects of urge and reward, particularly those measuring sub-second electroencephalogram (EEG) brain dynamics. To address these issues, we designed an EEG study to ask three questions: (1) How does urge develop? (2) What are EEG-correlates of blink suppression? (3) How does reward change brain dynamics related to urge suppression? This study examined healthy children (N=26, age 8-12 years) during blink suppression under three conditions: blink freely (i.e., no suppression), blink suppressed, and blink suppressed for reward. During suppression conditions, children used a joystick to indicate their subjective urge to blink. Results showed that (1) Half of the trials were associated with clearly-defined urge time course of ~7 s, which was accompanied by EEG delta (1-4 Hertz [Hz) power reduction localized at anterior cingulate cortex (ACC); (2) The EEG correlates of blink suppression was found in left prefrontal theta (4-8 Hz) power elevation; (3) Reward improved blink suppression performance while reducing the EEG delta power observed in ACC. We concluded that the empirically supported urge time course and underlying EEG modulations provide a sub-second chronospatial model of the brain dynamics during urge- and reward-mediated blink suppression.

Introduction

Clarifying the neural mechanisms of blink suppression in children is important for understanding how mental effort controls behavior, which may still be under developmental influences, unlike a comparable adult model. This understanding has critical value in child psychiatry, for example in designing a clinical behavioral training program for treating children with Tourette's syndrome (Woods and Himle, 2004; Greene et al., 2015). These studies reported clinically important findings that although tics had been considered as a result of biological disorder, operant contingencies using a reinforcer ($2 in Woods and Himle, 2004) could suppress tic behavior in children. However, the underlying neural mechanism in children remains unclear. Neuroimaging studies during urge suppression help to localize neural substrata and elucidate their dynamics corresponding to the mental processes. One of the earliest studies investigated 'air hunger' (or shortness of breath) and found activations in the mid to anterior right insula, a part of the limbic system (Banzett et al., 2000). The most well-studied experimental paradigm to date is blink suppression. Neuroimaging studies using PET on blink suppression reported activation in right insular cortex and anterior cingulate cortex (Lerner et al., 2009). Similarly, functional MRI activations in right insular cortex, right ventrolateral prefrontal cortex, and bilateral temporal gyri showed correlations with a hypothetical model for the time-course of urge. In the model, urge takes 60 s to build up to the peak, after which a blink occurs and is followed by another 15 s to release (Berman et al., 2012). The same group also studied the effect of neurofeedback training using a blink suppression task and reported changes in functional connectivity between anterior insula and medial frontal cortex (Berman et al., 2013). This study was one of several to support the now established relationship between blink suppression and the activation within the right insula.

In addition to insula, other interacting regions, which are mostly distributed in the frontal lobe, have also been implicated in urge suppression. For example, the right ventrolateral prefrontal cortex is another well-established region in response inhibition such as in the Go/No Go task and Stop Signal task (Aron et al., 2004, 2014). The right ventrolateral prefrontal and insular cortices are a part of circuit that maintains volitional suppression of behavior during an increasing sense of urge. A recent study on healthy adults reported the neural correlates of blink suppression to be in bilateral insula, sensorimotor, anterior prefrontal, parietal cortices, as well as subcortical regions including putamen and caudate (van der Salm et al., 2018). Another study investigated cough suppression after inhaling capsaicin solution (Mazzone et al., 2011). Regions

activated included bilateral insula, cingulate cortex, middle frontal gyrus, and posterior cingulate gyrus, which confirmed the involvement of insula in different types of suppression. Developmentally, adults showed more activation in widespread regions during blink suppression compared with children, but blink-suppression-related inhibition in posterior cingulate cortex was relatively comparable (Mazzone et al., 2010). Importantly, they reported bilateral dorsolateral prefrontal cortices (DLPFCs) and anterior cingulate cortex (ACC) to be key regions for both children and adults.

While there is converging evidence from neuroimaging studies, there are still unanswered questions. One critical question remaining is the temporal relationship between increased urge and its associated brain dynamics. As reviewed above, one fMRI study attempted to study temporal aspect of urge building (Berman et al., 2012). The major limitations in their study was that the hypothetical temporal model of building urge was heuristically determined without empirical data support. Moreover, BOLD signal does not have good temporal resolution compared with electrophysiological measures. In order to answer the question of the relation between urge and brain dynamics, modalities with high temporal resolution such as EEG or MEG are natural choices. However, as far as we know, there have been no EEG studies on the temporal relation between urge and brain dynamics. The other critical question remaining is how reward-facilitated blink suppression is represented in the typically developing brain. It is reported that reward enhances successful tic suppression (Woods and Himle, 2004; Greene et al., 2015). However, the neural mechanisms underlying this process are poorly understood. Clarification of this question is particularly important for enhancing behavioral interventions, which are often used for patients with Tourette Disorder.

In the present study, we conducted an EEG study of blink suppression performed by healthy control children. The following three questions were tested: (1) What is the time course of urge development? (2) What are the EEG-correlates of blink suppression? (3) How does reward change brain dynamics related to urge suppression? To investigate the temporal relation between building urge and brain dynamics, the children used a joystick as an ‘urgeometer’ to indicate their subjective experience of urge. Also, to investigate the effect of reward on urge suppression, there were three experimental conditions: 1. Blink Freely/No Suppression (No Supp), 2. Verbal Suppression (Supp), and 3. Suppression for Reward (Supp Rwd). The trials in the latter two conditions were subsequently separated into two subgroups based on urge (Urge High and Urge Low), and the interaction between urge and reward was tested.

Materials and Methods

Sample

Participants were 35 healthy control children between the ages of 8-12 years old who were recruited as a comparison group for a larger study on Tourette Disorder; data on the patient group will be reported separately. In order to ensure enough trials for the event-related EEG analysis, a minimum threshold of more than 20 blinks in NoSupp condition and 10 blinks in Supp and Supp Rwd conditions (conditions will be described later) was used. The final sample for EEG analysis consisted of 26 children (12 males, 14 females) with a mean age of 9.6 years (SD 1.5, range 8-12). The children were recruited from the community through radio and newspaper advertisements, community organizations, local schools, primary care physicians, and local clinics. After receiving verbal and written explanations of study requirements, and prior to any study procedures, all parents/participants provided written permission and informed consent/assent as approved by the Institutional Review Board.

Procedures

Subjects were excluded from participation if they were positive for any of the following: presence of any major Diagnostic and Statistical Manual (American Psychiatric Association, 2013) Axis I diagnosis or taking any type of psychoactive medication, head injury resulting in concussion, or estimated Full Scale IQ < 80. The absence of psychiatric diagnoses was confirmed using a semi-structured diagnostic interview, the Anxiety Disorder Interview Schedule, Child Version (ADIS) (Silverman et al., 2001), which was administered by trained and carefully supervised graduate level psychologists. Estimated intelligence (IQ) was assessed using the Wechsler Abbreviated Scale of Intelligence (WASI) (Weschler, 1999).

Task

There were three block-separated conditions: blink freely/no blink suppression (No Supp), verbal instruction for blink suppression (Supp), and blink suppression for reward (Supp Rwd). All children were instructed to blink freely during the No Supp block, while trying to suppress blinks during the two blink suppression blocks. During Supp Rwd, children were told that the computer would be counting how many blinks they were able to suppress, and that they would subsequently receive a reward for successful suppression. All children received $10 regardless of how many blinks they

exhibited. During the two blink suppression blocks, children used a custom joystick to indicate their subjective experience of urge for blinking by moving the stick forward when they felt the urge to blink. The joystick would revert back to the neutral condition automatically once pressure was released. The order of the three conditions were counterbalanced across subjects. There were other types of cognitive tasks in between the blink freely/suppression blocks, which will be presented elsewhere. Each block length was between 5-7 min.

EEG Recording

EEG signals were recorded using the Electrical Geodesics Incorporated (EGI) hardware and software with 128 Hydrogel electrodes that were embedded in a hydrocel net in an International 10/10 location system. Data were sampled at 1000 Hz and initially referenced to Cz. Electrode-skin impedance threshold was set at 50 kOhms per manufacturer standard for the high input impedance amplifier. Eye movements were monitored by electrodes placed on the outer canthus of each eye for horizontal movements (REOG, LEOG) and by electrodes above the eyes for vertical eye movements. Facial electromyography (EMG) leads were placed on the cheeks bilaterally over the zygomaticus major muscles to assist with detection of facial movements. Key head landmarks (nasion, inion, preauricular notches) and 3-D electrode locations were recorded (Polhemus, Inc.) to allow reconstruction of electrode positions on the scalp. All EEG data were recorded using the Lab Streaming Layer (https://github.com/sccn/labstreaminglayer), which allows integration of multiple data streams including EEG, high-definition video, joy-stick urgeometer, and experimental events.

EEG Preprocessing

Throughout the preprocessing, EEGLAB 14.1.2 (Delorme and Makeig, 2004) running under Matlab 2017b (The MathWorks, Inc., Natick, MA, USA) was used. Custom code was written as necessary. There were two central signal processing techniques: artifact subspace reconstruction (ASR) (Mullen et al., 2015; Chang et al., 2018, 2019; Gabard-Durnam et al., 2018; Blum et al., 2019; Plechawska-Wojcik et al., 2019), which is an offline version of data cleaning suits from BCILAB (Kothe and Makeig, 2013) (see Supplementary Material 7 for detail) and independent component analysis (ICA) (Bell and Sejnowski, 1995; Makeig et al., 1996, 1997, 2002). These two approaches are complementary in that ASR uses sliding-window principal component analysis (PCA)-

based subspace rejection and reconstruction so that it can address data non-stationarity such as infrequent short-lasting bursts by touching electrodes, for example, while ICA can find stationary processes and temporally maximally independent sources such as brain EEG sources as well as non-brain artifact sources like blink, eye movement, and facial and neck muscle activation by using more sophisticated, physiologically valid assumptions than PCA (Onton and Makeig, 2006; Delorme et al., 2012). After preprocessing the scalp recordings with these two algorithms, we analyzed event-related spectral perturbation (ERSP) on each anatomically defined source cluster to investigate time-frequency-space decomposed EEG power dynamics related to blink suppression. For full detail, see Supplementary Materials 1.

Identifying blinks

We developed an EEGLAB plugin *countBlinks()* for this project (available from https://sccn.ucsd.edu/eeglab/plugin_uploader/plugin_list_all.php) to manually annotate all the blinks during the tasks by visually examining the time-series data of the independent component (IC) representing blink/vertical eye movement. The principle in this blink identification is peak detection in the EOG-IC time series, hence the annotated markers refers to the highest-amplitude moment, rather than the onset, of a blink. The solution does not use an algorithm; an annotator judged whether the currently highlighted blink-induced-like EOG waveforms (typically 0.5-1.0 s long) should be labeled as blink or not for each of candidate waveform. When the data showed stereotypical blink-induced waveforms, annotating 2-3 blinks per second was possible due to the efficient GUI design. Several automated algorithms were tested out before developing our own solution, but their performances turned out to be often unsatisfactory particularly during blocks with suppression conditions. This was probably because participant’s physical effort to suppress the blinks prevented generation of stereotypical blink-induced EOG waveforms. Thus, we were motivated to instead use manual annotation in an efficient way.

Statistical testing

The full factorial design of the current study was 3 suppression factors (No Supp, Supp, Supp Rwd) x 2 urge factors (Urge High, Urge Low), all within-subject design. However, because urge was measured only for the suppression conditions, the No Supp condition did not have urge data. We determined three contrasts of interest; Contrast 1, main

effect of Suppression; Contrast 2, main effect of Urge; Contrast 3 main effect of Reward (Figure 1).

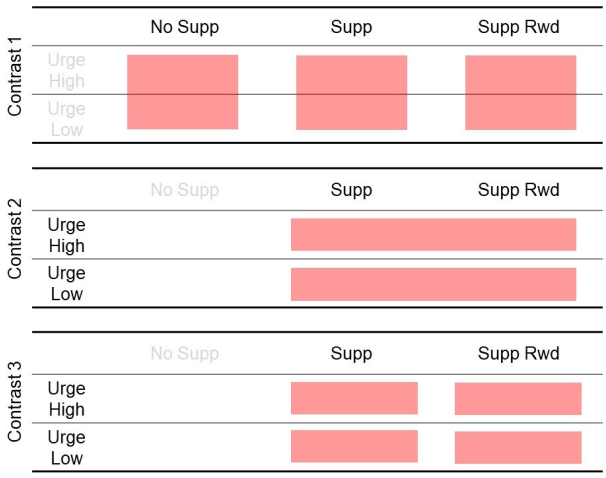

Figure 1. The factorial design of the current study. There were three contrasts for which statistical tests were performed. Note that the Contrast 2 and 3 include only two suppression conditions because urge data was not collected during 'No Supp' condition.

Repeated measures ANOVAs were performed for Contrasts 1 and 3, and paired t-test for Contrast 2, on each time-frequency pixel of the calculated ERSP tensor with the dimensions of 100 (frequencies, 1 to 55 Hz) x 252 (latency to blink ERP peak, -4030 to 1000 ms) x number_of_ICs (this varies from IC cluster to cluster) for 12 IC clusters. For multiple comparison correction for the 100 x 252 time-frequency points, weak family-wise error rate (wFWER) control was used (Groppe et al., 2011). *t*- or *F*-statistics values were computed for all time-frequency points and thresholded at $p < 0.001$ and $p < 0.005$ for Contrast 1 and Contrast 2, respectively. The true *mass of cluster*, which is the sum of absolute *t*- or *F*-statistics within a time-frequency point cluster, was computed for each cluster. Next, data labels were shuffled and the same procedure was applied, and the largest mass of cluster was taken to build distribution of surrogate mass of cluster. Finally, 99.9 and 99.5 percentiles of surrogate mass of cluster distribution was determined to be used as a threshold value for omnibus correction. Those true mass of cluster entries that showed larger values than the threshold values were declared to be statistically significant after wFWER control.

Results

Behavioral Data

The number of blinks was counted for each block and normalized into average counts per minute for each subject. The results were as follows: No Supp, M = 17.8 (SD 8.9); Supp, M = 10.7 (SD 6.2); Supp Rwd, M = 8.4 (SD 4.4). Paired t-tests across the three conditions confirmed significant reduction of blinks in the order of No Supp, Supp, and Supp Rwd (all $p < 0.001$, Figure 2). The result confirmed the validity of the experimental control over blink suppression. The distribution of other blinks relative to a blink is shown in Supplementary Material 4.

The grand-mean urgeometer time series (+/- 1SD) plotted separately for High and Low Urge conditions indicates urge peak was reached slightly earlier than the EOG-ERP peak latency. The peak latency for Urge High was found at -0.4 s relative to blink EOG-ERP peak. Next, the elbow point of the rising curve up to the peak was obtained using a two-line fitting bisection method to find the point where the residual from the two-line fitting is minimized. Relative to the EOG-ERP peak, the elbow point was found at -1.8 s. The result indicated that the urge increase rate is nonlinear, and it became steeper after -1.8 s. Finally, Urge Low showed a flat pattern, indicating that about half of the blinks (i.e., suppression failures) may have occurred with little to no urge experienced by participants.

For interest, we characterized impact of eye blinks and urge on sensor-level ERP and their ICA-decomposition. The results are summarized in Supplementary Material 2 and Supplementary Material 3, respectively.

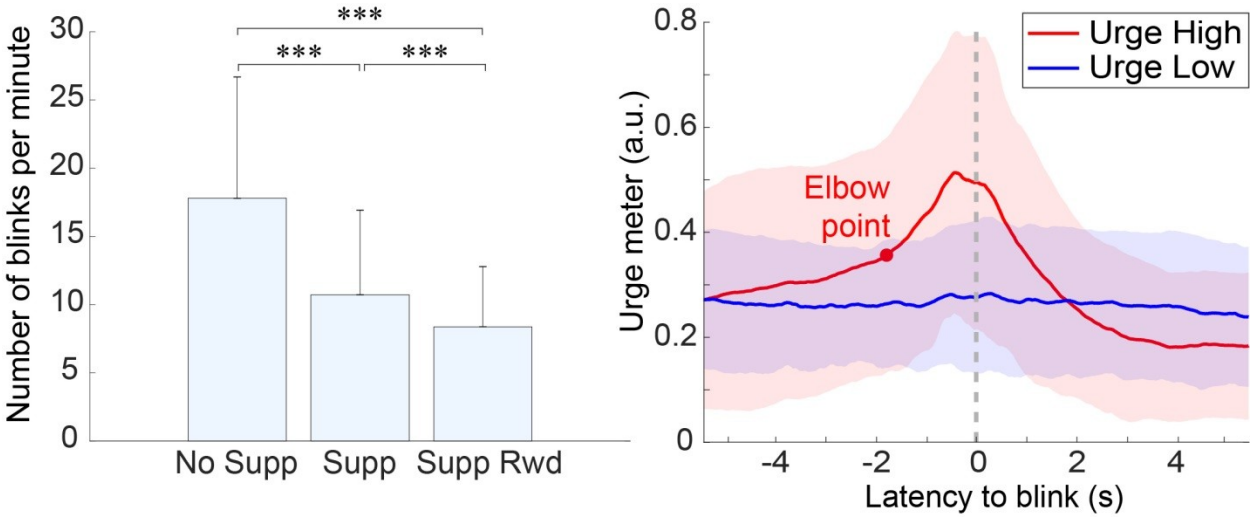

*Figure 2. Left, the group-mean number of blink counts for the condition Suppression. The error bar represents 1 SD. ***, $p < 0.001$ (Bonferroni corrected). Right, average*

time-course of urge input obtained from trials separated into Urge High and Low. The trials were separated into the two groups according to the single-trial urge time-series correlation with that of the within-subject mean. The red dot on the Urge High plot around -1.812 s point shows the optimum bisection point that separates the rise of the plot into two parts. The color shades in the plot indicates +/-1 SD.

General descriptive statistics about preprocessing, ICA-decomposed EEG, and multiple comparison correction

The total amount of variance reduction after all the preprocessing was: percent variance accounted for (PVAF) reduction, M = 99.7 %, SD = 0.3, range 98.6-99.9. This PVAF difference is the result from the following two stages of signal processing: reduction to 1.5-55 Hz bandpass filtering and ASR (M = 98.4, SD = 2.5, range 88.5-99.9); reduction due to the subsequent IC rejection (M = 74.4, SD = 13.3, range 38.5-96.7).

For the group-level analysis, 910/3224 qualified brain ICs were selected from the final sample of 26 participants who showed more than 20 blinks for No Supp and 10 blinks for Supp and Supp Rwd blocks, respectively. The number of brain ICs contributed from individual subjects was M = 35.0 (SD = 13.8, range 10-61). The optimum numbers of IC clusters based on the spatial coordinates of the dipoles were 12 and 14 for Silhouette and Davies-Bouldin, respectively. Calinski-Harabasz did not show an optimum point. To increase the chance of obtaining a higher number of unique subjects per cluster, we chose to generate 12 IC clusters. Mean scalp topography, power spectral density, and Event-related spectral perturbation (ERSP) within the cluster and across all the conditions are shown in Figure 3 to show a general outline of the group-level clustered ICs.

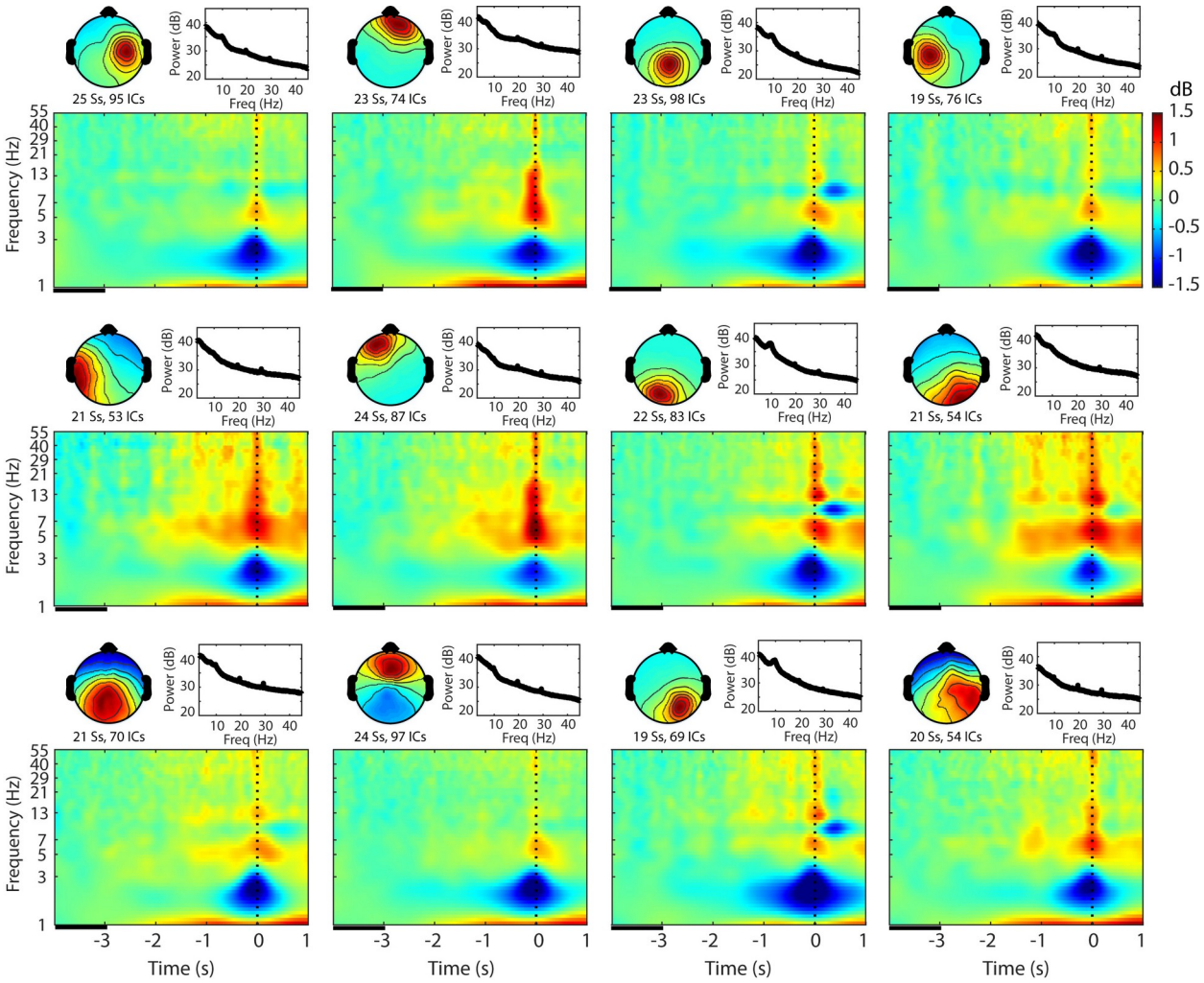

Figure 3. Cluster-mean scalp topography, power spectral density, and Event-related spectral perturbation (ERSP) for each of the 12 clusters determined by Silhouette analysis and averaged across all the conditions. This figure shows general outline of the whole-brain data right after group-level independent component (IC) clustering. The graph scales are identical across the clusters. In the time-frequency plots, baseline period is indicated as black line between -4 to -3 s relative to blink onset. Ss, subjects; ICs, independent components.

Main effect Suppression

The statistical test on the main effect Suppression revealed that the IC cluster localized near the left prefrontal cluster differentiated No Supp vs. Supp (with or without Rwd) (Figure 4). The location corresponds with previously reported DLPFC activation during eye-blink inhibition (Mazzone et al., 2010). The time-frequency analysis revealed theta-

band (4-8Hz) power increase for suppression conditions that started approximately -1.5 s prior to blink, which is a failure of blink suppression. These results may reflect increased effort to suppress blinks against increasing urge. Thus, we replicated anatomical location from the previous fMRI study, and furthermore succeeded in characterizing the modulation of brain dynamics as elevation of theta power during suppression with sub-second time resolution. The same comparison for the rest of the IC clusters are shown in Supplementary Materials 6.

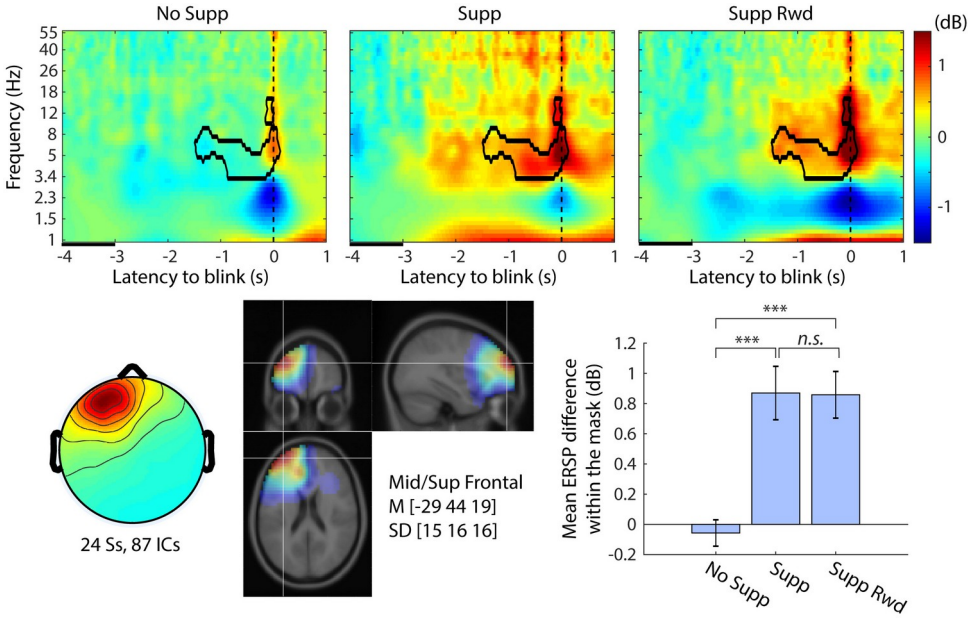

*Figure 4. Event-related spectral perturbation (ERSP) plots for main effect Suppression (No Supp, Supp, Supp Rwd) in the left prefrontal independent component (IC) cluster. The contour mask in the time-frequency plots indicates p < 0.001 after controlling weak family-wise error rate (wFWER). Top row, ERSP for No Supp, Supp, and Supp Rwd. Baseline period is indicated as black line between -4 to -3 s relative to blink onset. Bottom left, cluster-mean IC scalp topography. Bottom center, cluster-mean dipole density with FWHM = 20 mm and the centroid coordinate in the MNI template head. Bottom right, the mean ERSP values with SE within the significance mask compared across conditions. *** p < 0.001.*

Main effect Urge

The statistical test on the main effect Urge revealed that the IC cluster localized near the anterior cingulate cluster differentiated Urge Low vs. Urge High (Figure 5). The location corresponds with a previously reported ACC activation during eye-blink

inhibition (Mazzone et al., 2010). The time-frequency analysis revealed that subjective sense of urge was associated with power decrease in delta band (1-4 Hz) starting from 1 s prior to blinks. When we compare this delta-band ERSP suppression with the time-course of the urgeometer data for Urge High, we notice that the non-significant left tail of the delta-band suppression in Urge High starting from -3 s may be corresponding to gradual increase of urgeometer values that started from -4 s. Also, the elbow point determined in the urgeometer data for Urge High (-1.8 s) seems to precede the ERSP difference (-1 s), but it is positioned in the middle of long left tail of this early non-significant portion of the continuum. Closer inspection of the significance mask indicates that the midpoint of the mask in time is not on zero but a few hundred millisecond prior to zero, which may correspond to the fact that the urgometer peak was registered at -0.4 s. The significance threshold of $p < 0.005$ is arbitrary, and as such exact agreement between the behavioral data and the EEG data in their time-courses may or may not occur, however, it is possible to see, in a general sense, the temporal correspondence between the urgeometer behavioral data and EEG modulations. The same comparison for the rest of the IC clusters are shown in Supplementary Materials 7.

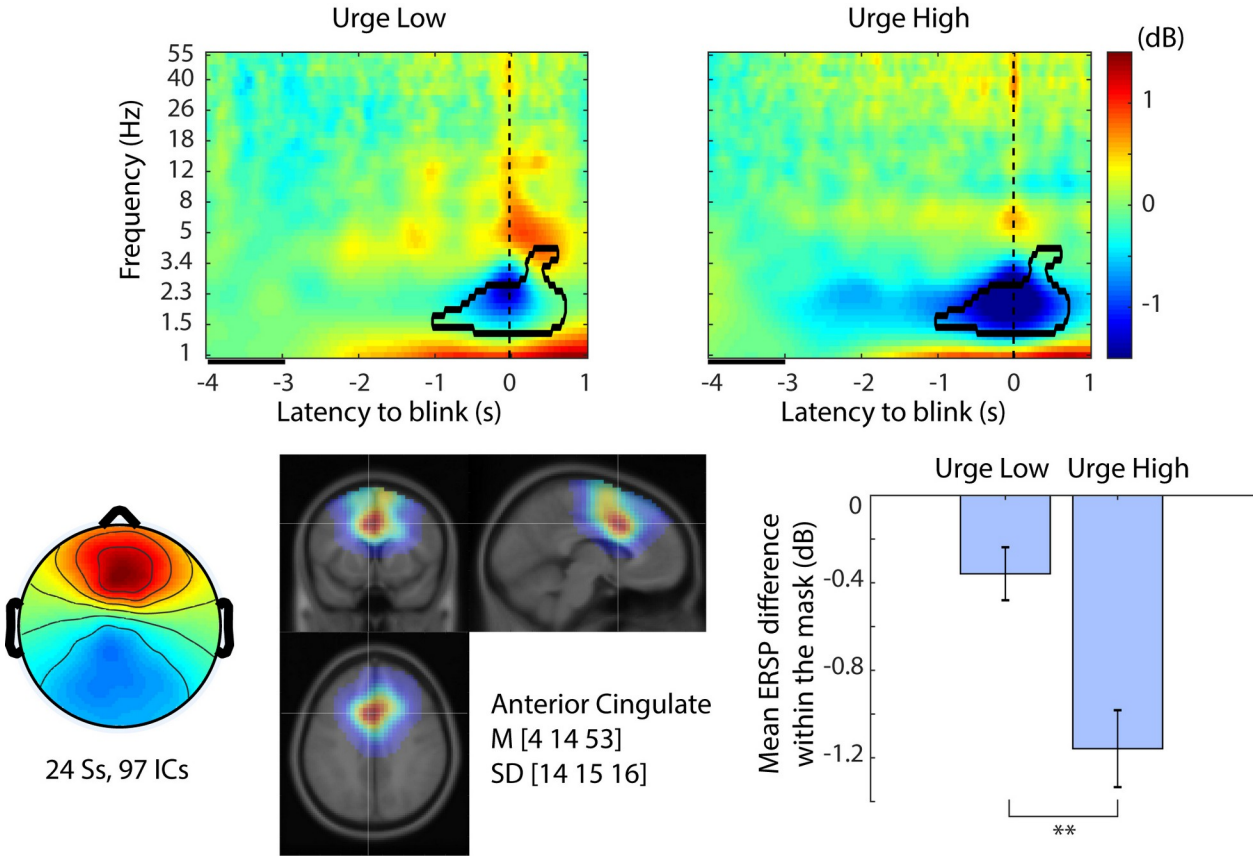

*Figure 5. Event-related spectral perturbation (ERSP) plots for main effect Urge (Urge Low, Urge High) in the anterior cingulate independent component (IC) cluster. The contour mask in the time-frequency plots indicates p < 0.005 after controlling weak family-wise error rate (wFWER). Top row, ERSP for Urge Low and Urge high. Baseline period is indicated as black line between -4 to -3 s relative to blink onset. Bottom left, cluster-mean IC scalp topography. Bottom center, cluster-mean dipole density with FWHM = 20 mm and the centroid coordinate in the MNI template head. Bottom right, the mean ERSP values with SE within the significance mask compared across conditions. ** p < 0.005.*

Interaction Urge and Reward

The same ACC cluster that showed the main effect of Urge reported above also showed significant interaction between Urge and Reward. While suppression of the delta band (1-4 Hz) power was associated with higher urge, the introduction of reward diminished this difference between Urge High and Urge Low; the results are shown in Figure 6. Interestingly, the significance masks from the urge (Figure 5) and urge x reward (Fig. 6) do not overlap and the latency starts 2 s earlier in the latter analysis. This suggests that offering a Reward for successful suppression equalizes the response of the ACC region, regardless of urge intensity. It is also noteworthy that the significant interaction continued after blink onset, indicating that the ACC region may also be involved in post-blink (i.e., suppression failure) processing, such as monitoring and evaluation. For interest, in order to minimize the effect of post-blink brain dynamics, we truncated the mask at 0 s and performed the same statistics. The result still showed the same pattern as shown in Figure 6 bottom right, confirming that the obtained result is valid for the suppression period (data not shown). When using weak FWER correction, this operation violates the assumption of the cluster-level correction so this test is limited to being a confirmatory process only.

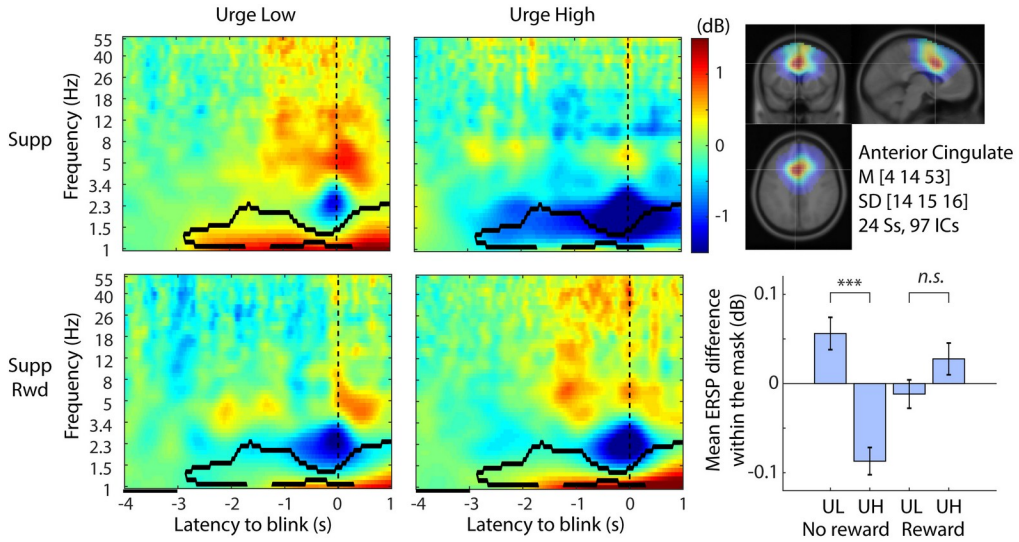

*Figure 6. Event-related spectral perturbation (ERSP) plots for interaction Urge and Reward in the anterior cingulate independent component (IC) cluster. The contour mask in the time-frequency plots indicates p < 0.001 after controlling weak family-wise error rate (wFWER). Left two columns indicates ERSPs for the 2 x 2 conditions. Baseline period is indicated as black line between -4 to -3 s relative to blink onset. Bottom left, cluster-mean IC scalp topography. Top right, cluster-mean dipole density with FWHM = 20 mm and the centroid coordinate in the MNI template head. Bottom right, the mean ERSP values with SE within the significance mask compared across conditions. *** p < 0.001.* UL, Urge Low; UH, Urge High.

Discussion

In the current study, we asked three research questions: (1) How does urge develop? (2) What are the EEG correlates of blink suppression? (3) How does reward change brain dynamics related to urge suppression? Let us describe the answers to each of these questions: (1) There are at least two subtypes of urge development, Urge High and Urge Low. Urge High trials showed a well-defined waveform that starts to rise -5 s relative to blink, while Urge Low trials did not show much modulation; (2) Blink suppression was associated with EEG theta band power increase near or in the left dorsolateral prefrontal cortex (DLPFC); and (3) Reward suppressed urge-related EEG delta band power decrease near or in the anterior cingulate cortex (ACC). Below, we will discuss details and significance of the results.

Our results showed that trials grouped as Urge High showed a relatively slow time constant that started to rise from -5 s before a blink. At -1.8 s, the increase

became steeper. At -0.4 s, the urge reached the peak. Around 2 s, it returned to baseline, and subsequently decreased below baseline (Figure 2). In a prior fMRI study, a 1-minute block-wise hemodynamic response model with linear increase toward the urge peak was used as a block-design regressor (Berman et al., 2012). However, this temporal model was designed heuristically and was not supported by empirical data. As far as we know, this is the first data to show the time course of building urge leading to a suppression failure. We also found non-linearity of the urge increase, with which we may be able to model building urge more realistically. The result not only improves our understanding of urge time course but the temporal kernel we obtained in this study may be used in fMRI studies to estimate BOLD signal changes correlated with internal urge dynamics.

The separation of Urge High and Urge Low, defined by single-trial correlation to their mean value, was an ad-hoc decision as a part of data mining. The validity of this decision can be argued for two reasons. The first reason is that the relation between urge and suppression failure is not necessarily established. In a study of tic suppression, which is considered an analogue of blink suppression (van der Salm et al., 2018), it was reported that subjective ability to self-monitor urge increased with age (Banaschewski et al., 2003). This suggests that younger children may not have developed the ability to monitor urge, and failure of suppression may suddenly happen before becoming aware of the urge. Under this hypothetical uncertainty on reliability of self-report, separating single trials of suppression failures into subgroups of with and without self-report seems a valid first step to analyze the behavioral variance. The second reason is that the urgeometer time-series data for Urge Low and High indeed became separated into two distinguishable curves. The result plot seems to support the possibility that the (hidden) distribution of urge across single trials is rather binary, urge present or absent, than Gaussian. Note that the joystick we used may have had relatively small range of angle between neutral and maximum stick tilt, which could have made analogue resolution of the self-reported urge value limited. However, even if the input from the analogue joystick was effectively used as binary input, their statistical distribution across trials and participants should still be able to be studied as continuous probabilistic distribution. The rather binary urge distribution, which seems to have effectively two status, namely on and off, also seems to explain why taking a simple mean across all the trials is not a good idea here. Our exploratory blink ERP analysis also showed lower peak amplitude in blink ERP, suggesting that blink behavior could be different when urge levels are different. It leads us to speculate that blinks with low urge may be

produced in more involuntary and reflexive way, hence they were faster and lighter than blinks with higher urge. Future studies on heterogeneity of single-trial self-reported urge expression with different age groups is awaited.

In the ERSP analysis, we focused on the pre-blink period during which blink suppression was still successfully maintained but about to collapse in a few seconds. The left prefrontal region showed distinctive EEG power increase prior to the blink during suppression conditions. The involvement of prefrontal regions (dorsolateral prefrontal cortex, DLPFC) in voluntary inhibition task has been reported repeatedly (Lerner et al., 2009; Mazzone et al., 2010; Aron et al., 2014). Our finding suggest that left prefrontal power increase is one of the EEG correlates of behavioral suppression, which is in line with these neuroimaging studies. Furthermore, our result provides rich time-frequency information. For example, we found this elevation started about -1.5 s to the blink with the present threshold. The urgeometer data showed that the urge increase rate changed at around -1.8 s, which seems to fit well with the ERSP time course. The data also showed that the EEG power increase was in the theta band (4-8 Hz), which suggests functional separation from, for example, the ACC region that showed EEG power decrease in the delta band (1-4 Hz) during the overlapping pre-blink period.

Analysis on main effect Urge revealed involvement of regions near anterior cingulate cortex (ACC), and Urge High was associated with deeper EEG power suppression compared with baseline period than Urge Low. ACC has been associated with various types of urges such as itch (Hsieh et al., 1994), voiding of urine (Kuhtz-Buschbeck et al., 2005; Griffiths et al., 2007), coughing (Mazzone et al., 2007; Leech et al., 2013), and smoking (Brody et al., 2004). Importantly, the same ACC cluster showed that subjective urge was modulated by availability of reward. This result was in line with our prediction that ACC is involved in subjective feeling, response coordination, self-monitoring, assessment of motivational valence, and initiation of motor actions (Medford and Critchley, 2010). ACC has been known to be a region where regulatory and executive processes interact (Paus, 2001). Involvement of ACC was also reported in a previous blink suppression study (Lerner et al., 2009) and antisaccade study (Milea et al., 2003). Not only did our scalp-recorded EEG results replicate these findings, our results showed for the first time sub-second temporal dynamics of how reward availability changes brain dynamics during subjective urge in the ACC region. The pattern of the interaction indicated that when reward is available, the urge-related ERSP power decrease was equalized between Urge Low and Urge High compared with the no

reward condition. This may indicate that enhanced motivation by reward availability worked as a reinforcer of the top-down control over urge. This view seems to be in harmony with a network view of ACC together with insula, which we will discuss below.

ACC and insula are functionally closely related to each other. Both ACC and insula commonly contain von Economo neurons (Allman et al., 2010), which are large bipolar neurons that are unique to these regions and also unique to great apes and humans. There is anatomical evidence that ACC, specifically Brodmann area 24 here, has reciprocal connection with insular cortex (Mesulam and Mufson, 1982; Vogt and Pandya, 1987), and this connection may be mediated by von Economo neurons (Craig, 2009). Thanks to this reciprocity, not only does insula integrate sensory information to generate awareness, which is then transferred to ACC for evaluating with various other information, making decisions, and initiating motor commands (feedforward connection), but also the result of the processing in ACC may be back-projected to insula to modulate how subjective awareness is formed (Medford and Critchley, 2010) (feedback connection). This view seems to be supported by empirical evidence that the placebo effect for antitussive therapies is generally substantial, but it turned out to be associated with modulation in activation of a cortical network including ACC and insula (Leech et al., 2013). The result indicates that the ACC-insula network was one of the major brain regions that received modulation just by top-down belief that lead to change in behavior. We speculate that reward availability in our study might be related to the same network, and ACC may have played a critical role in changing the behavior of blink suppression when reward was available.

The current finding may have clinical value for, for example, designing a behavioral training program for children with Tourette's syndrome (Woods and Himle, 2004; Greene et al., 2015). Our results provided evidence of neural substrata underlying the behavioral suppression. Together with other literatures of neuroimaging studies, our results can provide spatio-temporally resolved neural mechanism of behavioral suppression. Particularly, the parallel time courses of behavioral and electrophysiological dynamics toward suppression failure we showed in this study seem capable of providing a spatio-temporal target for treatment using transcranial magnetic stimulation (TMS) for tic patients. Future studies toward this direction is awaited.

Limitation

The results of this study are the first of its kind and as such should be considered preliminary until independent replication occurs. Additional limitations are noted as

follows. Presence of blink and related muscle artifact in EEG recording typically creates critical limitation. We addressed this issue by using two approaches. One of the approaches was to set the main time window of analysis prior to the blink onset. In fact, eye blink in this study indicates the offset of the time window of interest. The other approach was to employ independent component (IC) modeling approach (Onton and Makeig, 2006) rather than scalp electrode signal analysis. We performed a post-hoc simulation study, which can be found in Supplementary Material 5.

The use of the urgeometer in the current study can be argued. The ability to self-monitor urge depends on age (Banaschewski et al., 2003). In addition, using the urgeometer may impose multi-tasking of self-monitoring and motor execution, which may have interfered with suppression performance and associated brain dynamics. Care needs to be taken when we interpret the ERSP differences between No Supp (no urgeometer use) and other Supp conditions (urgeometer used).

We relied on suppression-breaking blinks to define the suppression period. For this reason, we needed to exclude remove several participants with fewer number of blinks. It may seem possible to define ‘successful suppression’ when urgeometer showed high value but no blink followed. But this approach has two problems: 1) We do not know whether urge could disappear with continued suppression; 2) an additional condition is necessary to consider in which the urgeometer is used irrespective of urge to counterbalance the brain dynamics related to motor planning and execution. Future studies with the suggested conditions may be helpful to validate the use of the urgeometer.

Due to known dependencies of scalp EEG recording on cytoarchitecture, source distance and geometry (Nunez and Srinivasan, 2006), our main results were limited to cortical sources close to the surface and contribution of deeper sources such as insula was not detected. Moreover, in the case of insula it is also reported that active source area spreads rapidly to surrounding structures (Sun et al., 2015), which makes it difficult to form a temporally stable active cortical patch that can be detected at scalp recording. In epilepsy studies, differentiation of insular seizures from temporal, parietal, and frontal lobe seizures (Isnard et al., 2004; Nguyen et al., 2009) was not possible, suggesting that both interictal and ictal recordings might fail to display epileptiform discharges for insular seizures (Desai et al., 2011; Ryvlin and Picard, 2017). Thus, it is generally hard to obtain insular activity with scalp EEG recording. For interpreting the current results, however, there are a large number of anatomical and neuroimaging studies on the insula and ACC-insula network. As we demonstrated above, using the

wealth of literature to interpolate the lack of insular and basal contributions seems necessary to interpret the current EEG result in the context of neuroimaging studies on blink suppression.

Conclusion

We demonstrated that 1) Blink suppression was associated with EEG theta band power increase near or in the left DLPFC; 2) Reward improved suppression performance, and Reward suppressed urge-related EEG delta band power decrease near or in the ACC; 3) Real-time self-reported urge has single-peaked time-course longer than 7 s (and peaking at -.4 s) , but this applies only to half of failed suppression trials.

Figure Legend

Figure 1. The factorial design of the current study. There were three contrasts for which statistical tests were performed. Note that the Contrast 2 and 3 include only two suppression conditions because urge data was not collected during 'No Supp' condition.

*Figure 2. Left, the group-mean number of blink counts for the condition Suppression. The error bar represents 1 SD. ***, p < 0.001 (Bonferroni corrected). Right, average time-course of urge input obtained from trials separated into Urge High and Low. The trials were separated into the two groups according to the single-trial urge time-series correlation with that of the within-subject mean. The red dot on the Urge High plot around -1.812 s point shows the optimum bisection point that separates the rise of the plot into two parts. The color shades in the plot indicates +/-1 SD.*

Figure 3. Cluster-mean scalp topography, power spectral density, and Event-related spectral perturbation (ERSP) for each of the 12 clusters determined by Silhouette analysis and averaged across all the conditions. This figure shows general outline of the whole-brain data right after group-level independent component (IC) clustering. The graph scales are identical across the clusters. In the time-frequency plots, baseline period is indicated as black line between -4 to -3 s relative to blink onset. Ss, subjects; ICs, independent components.

*Figure 4. Event-related spectral perturbation (ERSP) plots for main effect Suppression (No Supp, Supp, Supp Rwd) in the left prefrontal independent component (IC) cluster. The contour mask in the time-frequency plots indicates p < 0.001 after controlling weak family-wise error rate (wFWER). Top row, ERSP for No Supp, Supp, and Supp Rwd. Baseline period is indicated as black line between -4 to -3 s relative to blink onset. Bottom left, cluster-mean IC scalp topography. Bottom center, cluster-mean dipole density with FWHM = 20 mm and the centroid coordinate in the MNI template head. Bottom right, the mean ERSP values with SE within the significance mask compared across conditions. *** p < 0.001.*

*Figure 5. Event-related spectral perturbation (ERSP) plots for main effect Urge (Urge Low, Urge High) in the anterior cingulate independent component (IC) cluster. The contour mask in the time-frequency plots indicates p < 0.005 after controlling weak family-wise error rate (wFWER). Top row, ERSP for Urge Low and Urge high. Baseline period is indicated as black line between -4 to -3 s relative to blink onset. Bottom left, cluster-mean IC scalp topography. Bottom center, cluster-mean dipole density with FWHM = 20 mm and the centroid coordinate in the MNI template head. Bottom right, the mean ERSP values with SE within the significance mask compared across conditions. ** p < 0.005.*

*Figure 6. Event-related spectral perturbation (ERSP) plots for interaction Urge and Reward in the anterior cingulate independent component (IC) cluster. The contour mask in the time-frequency plots indicates p < 0.001 after controlling weak family-wise error rate (wFWER). Left two columns indicates ERSPs for the 2 x 2 conditions. Baseline period is indicated as black line between -4 to -3 s relative to blink onset. Bottom left, cluster-mean IC scalp topography. Top right, cluster-mean dipole density with FWHM = 20 mm and the centroid coordinate in the MNI template head. Bottom right, the mean ERSP values with SE within the significance mask compared across conditions. *** p < 0.001.* UL, Urge Low; UH, Urge High.

Bibliography

Allman JM, Tetreault NA, Hakeem AY, Manaye KF, Semendeferi K, Erwin JM, Park S, Goubert V, Hof PR (2010) The von Economo neurons in frontoinsular and anterior cingulate cortex in great apes and humans. Brain Struct Funct 214:495–517.

American Psychiatric Association (2013) Diagnostic And Statistical Manual Of Mental Disorders, 5th Edition, 5th ed. Washington, D.C: American Psychiatric Publishing.

Aron AR, Robbins TW, Poldrack RA (2004) Inhibition and the right inferior frontal cortex. Trends Cogn Sci (Regul Ed) 8:170–177.

Aron AR, Robbins TW, Poldrack RA (2014) Inhibition and the right inferior frontal cortex: one decade on. Trends Cogn Sci (Regul Ed) 18:177–185.

Banaschewski T, Woerner W, Rothenberger A (2003) Premonitory sensory phenomena and suppressibility of tics in Tourette syndrome: developmental aspects in children and adolescents. Dev Med Child Neurol 45:700–703.

Banzett RB, Mulnier HE, Murphy K, Rosen SD, Wise RJ, Adams L (2000) Breathlessness in humans activates insular cortex. Neuroreport 11:2117–2120.

Bell AJ, Sejnowski TJ (1995) An information-maximization approach to blind separation and blind deconvolution. Neural Comput 7:1129–1159.

Berman BD, Horovitz SG, Hallett M (2013) Modulation of functionally localized right insular cortex activity using real-time fMRI-based neurofeedback. Front Hum Neurosci 7:638.

Berman BD, Horovitz SG, Morel B, Hallett M (2012) Neural correlates of blink suppression and the buildup of a natural bodily urge. Neuroimage 59:1441–1450.

Blum S, Jacobsen NSJ, Bleichner MG, Debener S (2019) A riemannian modification of artifact subspace reconstruction for EEG artifact handling. Front Hum Neurosci 13:141.

Brody AL, Mandelkern MA, Lee G, Smith E, Sadeghi M, Saxena S, Jarvik ME, London ED (2004) Attenuation of cue-induced cigarette craving and anterior cingulate cortex activation in bupropion-treated smokers: a preliminary study. Psychiatry Res 130:269–281.

Chang C-Y, Hsu S-H, Pion-Tonachini L, Jung T-P (2018) Evaluation of artifact subspace reconstruction for automatic EEG artifact removal. Conf Proc IEEE Eng Med Biol Soc 2018:1242–1245.

Chang C-Y, Hsu S-H, Pion-Tonachini L, Jung T-P (2019) Evaluation of Artifact Subspace Reconstruction for Automatic Artifact Components Removal in Multi-channel EEG Recordings. IEEE Trans Biomed Eng.

Craig ADB (2009) How do you feel--now? The anterior insula and human awareness. Nat Rev Neurosci 10:59–70.

Delorme A, Makeig S (2004) EEGLAB: an open source toolbox for analysis of single-trial EEG dynamics including independent component analysis. J Neurosci Methods 134:9–21.

Delorme A, Palmer J, Onton J, Oostenveld R, Makeig S (2012) Independent EEG sources are dipolar. PLoS One 7:e30135.

Desai A, Jobst BC, Thadani VM, Bujarski KA, Gilbert K, Darcey TM, Roberts DW (2011) Stereotactic depth electrode investigation of the insula in the evaluation of medically intractable epilepsy. J Neurosurg 114:1176–1186.

Gabard-Durnam LJ, Mendez Leal AS, Wilkinson CL, Levin AR (2018) The Harvard Automated Processing Pipeline for Electroencephalography (HAPPE): Standardized Processing Software for Developmental and High-Artifact Data. Front Neurosci 12:97.

Greene DJ, Koller JM, Robichaux-Viehoever A, Bihun EC, Schlaggar BL, Black KJ (2015) Reward enhances tic suppression in children within months of tic disorder onset. Dev Cogn Neurosci 11:65–74.

Griffiths D, Tadic SD, Schaefer W, Resnick NM (2007) Cerebral control of the bladder in normal and urge-incontinent women. Neuroimage 37:1–7.

Groppe DM, Urbach TP, Kutas M (2011) Mass univariate analysis of event-related brain potentials/fields I: a critical tutorial review. Psychophysiology 48:1711–1725.

Hsieh JC, Hägermark O, Ståhle-Bäckdahl M, Ericson K, Eriksson L, Stone-Elander S, Ingvar M (1994) Urge to scratch represented in the human cerebral cortex during itch. J Neurophysiol 72:3004–3008.

Isnard J, Guénot M, Sindou M, Mauguière F (2004) Clinical manifestations of insular lobe seizures: a stereo-electroencephalographic study. Epilepsia 45:1079–1090.

Kothe CA, Makeig S (2013) BCILAB: a platform for brain-computer interface development. J Neural Eng 10:056014.

Kuhtz-Buschbeck JP, van der Horst C, Pott C, Wolff S, Nabavi A, Jansen O, Jünemann KP (2005) Cortical representation of the urge to void: a functional magnetic resonance imaging study. J Urol 174:1477–1481.

Leech J, Mazzone SB, Farrell MJ (2013) Brain activity associated with placebo suppression of the urge-to-cough in humans. Am J Respir Crit Care Med 188:1069–1075.

Lerner A, Bagic A, Hanakawa T, Boudreau EA, Pagan F, Mari Z, Bara-Jimenez W, Aksu M, Sato S, Murphy DL, Hallett M (2009) Involvement of insula and cingulate cortices in control and suppression of natural urges. Cereb Cortex 19:218–223.

Makeig S, Bell A, Jung T-P, Sejnowski T (1996) Independent component analysis of electroencephalographic data. Advances in Neural Information Processing Systems 8:145–151.

Makeig S, Jung TP, Bell AJ, Ghahremani D, Sejnowski TJ (1997) Blind separation of auditory event-related brain responses into independent components. Proc Natl Acad Sci USA 94:10979–10984.

Makeig S, Westerfield M, Jung TP, Enghoff S, Townsend J, Courchesne E, Sejnowski TJ (2002) Dynamic brain sources of visual evoked responses. Science 295:690–694.

Mazzone L, Yu S, Blair C, Gunter BC, Wang Z, Marsh R, Peterson BS (2010) An FMRI study of frontostriatal circuits during the inhibition of eye blinking in persons with Tourette syndrome. Am J Psychiatry 167:341–349.

Mazzone SB, Cole LJ, Ando A, Egan GF, Farrell MJ (2011) Investigation of the neural control of cough and cough suppression in humans using functional brain imaging. J Neurosci 31:2948–2958.

Mazzone SB, McLennan L, McGovern AE, Egan GF, Farrell MJ (2007) Representation of capsaicin-evoked urge-to-cough in the human brain using functional magnetic resonance imaging. Am J Respir Crit Care Med 176:327–332.

Medford N, Critchley HD (2010) Conjoint activity of anterior insular and anterior cingulate cortex: awareness and response. Brain Struct Funct 214:535–549.

Mesulam MM, Mufson EJ (1982) Insula of the old world monkey. III: Efferent cortical output and comments on function. J Comp Neurol 212:38–52.

Milea D, Lehéricy S, Rivaud-Péchoux S, Duffau H, Lobel E, Capelle L, Marsault C, Berthoz A, Pierrot-Deseilligny C (2003) Antisaccade deficit after anterior cingulate cortex resection. Neuroreport 14:283–287.

Mullen TR, Kothe CAE, Chi YM, Ojeda A, Kerth T, Makeig S, Jung T-P, Cauwenberghs G (2015) Real-Time Neuroimaging and Cognitive Monitoring Using Wearable Dry EEG. IEEE Trans Biomed Eng 62:2553–2567.

Nguyen DK, Nguyen DB, Malak R, Leroux J-M, Carmant L, Saint-Hilaire J-M, Giard N, Cossette P, Bouthillier A (2009) Revisiting the role of the insula in refractory partial epilepsy. Epilepsia 50:510–520.

Nunez PL, Srinivasan R (2006) Electric fields of the brain. Oxford University Press.

Onton J, Makeig S (2006) Information-based modeling of event-related brain dynamics. Prog Brain Res 159:99–120.

Paus T (2001) Primate anterior cingulate cortex: where motor control, drive and cognition interface. Nat Rev Neurosci 2:417–424.

Plechawska-Wojcik M, Kaczorowska M, Zapala D (2019) The artifact subspace reconstruction (ASR) for EEG signal correction. A comparative study. In: Information systems architecture and technology: proceedings of 39th international conference on information systems architecture and technology – ISAT 2018: part II (Świątek J, Borzemski L, Wilimowska Z, eds), pp 125–135 Advances in intelligent systems and computing. Cham: Springer International Publishing.

Ryvlin P, Picard F (2017) Invasive investigation of insular cortex epilepsy. J Clin Neurophysiol 34:328–332.

Silverman WK, Saavedra LM, Pina AA (2001) Test-retest reliability of anxiety symptoms and diagnoses with the Anxiety Disorders Interview Schedule for DSM-IV: child and parent versions. J Am Acad Child Adolesc Psychiatry 40:937–944.

Sun T, Wang F, Cui J (2015) Insular cortex and insular epilepsy. J Neurol Neurosci 06.

van der Salm SMA, van der Meer JN, Cath DC, Groot PFC, van der Werf YD, Brouwers E, de Wit SJ, Coppens JC, Nederveen AJ, van Rootselaar A-F, Tijssen MAJ (2018) Distinctive tics suppression network in Gilles de la Tourette syndrome distinguished from suppression of natural urges using multimodal imaging. Neuroimage Clin 20:783–792.

Vogt BA, Pandya DN (1987) Cingulate cortex of the rhesus monkey: II. Cortical afferents. J Comp Neurol 262:271–289.

Weschler D (1999) Wechsler Abbreviated Scale of Intelligence. San Antonio, TX: The Psychological Corporation.

Woods DW, Himle MB (2004) Creating tic suppression: comparing the effects of verbal instruction to differential reinforcement. J Appl Behav Anal 37:417–420.

Makeig S, Gramann K, Jung T-P, Sejnowski TJ, Poizner H (2009) Linking brain, mind and behavior. Int J Psychophysiol 73:95–100.

Makeig S, Jung TP, Bell AJ, Ghahremani D, Sejnowski TJ (1997) Blind separation of auditory event-related brain responses into independent components. Proc Natl Acad Sci USA 94:10979–10984.

Makeig S, Westerfield M, Jung TP, Enghoff S, Townsend J, Courchesne E, Sejnowski TJ (2002) Dynamic brain sources of visual evoked responses. Science 295:690–694.

Mazzone L, Yu S, Blair C, Gunter BC, Wang Z, Marsh R, Peterson BS (2010) An FMRI study of frontostriatal circuits during the inhibition of eye blinking in persons with Tourette syndrome. Am J Psychiatry 167:341–349.

Mazzone SB, Cole LJ, Ando A, Egan GF, Farrell MJ (2011) Investigation of the neural control of cough and cough suppression in humans using functional brain imaging. J Neurosci 31:2948–2958.

Mazzone SB, McLennan L, McGovern AE, Egan GF, Farrell MJ (2007) Representation of capsaicin-evoked urge-to-cough in the human brain using functional magnetic resonance imaging. Am J Respir Crit Care Med 176:327–332.

Medford N, Critchley HD (2010) Conjoint activity of anterior insular and anterior cingulate cortex: awareness and response. Brain Struct Funct 214:535–549.

Mesulam MM, Mufson EJ (1982) Insula of the old world monkey. III: Efferent cortical output and comments on function. J Comp Neurol 212:38–52.

Milea D, Lehéricy S, Rivaud-Péchoux S, Duffau H, Lobel E, Capelle L, Marsault C, Berthoz A, Pierrot-Deseilligny C (2003) Antisaccade deficit after anterior cingulate cortex resection. Neuroreport 14:283–287.

Mullen TR, Kothe CAE, Chi YM, Ojeda A, Kerth T, Makeig S, Jung T-P, Cauwenberghs G (2015) Real-Time Neuroimaging and Cognitive Monitoring Using Wearable Dry EEG. IEEE Trans Biomed Eng 62:2553–2567.

Nguyen DK, Nguyen DB, Malak R, Leroux J-M, Carmant L, Saint-Hilaire J-M, Giard N, Cossette P, Bouthillier A (2009) Revisiting the role of the insula in refractory partial epilepsy. Epilepsia 50:510–520.

Nunez PL, Srinivasan R (2006) Electric fields of the brain. Oxford University Press.

Onton J, Makeig S (2006) Information-based modeling of event-related brain dynamics. Prog Brain Res 159:99–120.

Oostenveld R, Fries P, Maris E, Schoffelen J-M (2011) FieldTrip: Open source software for advanced analysis of MEG, EEG, and invasive electrophysiological data. Comput Intell Neurosci 2011:156869.

Palmer J, Kreutz-delgado K, Makeig S (2016) AMICA: An Adaptive Mixture of Independent Component Analyzers with Shared Components. https://sccn.ucsd.edu/~jason/amica_a.pdf

Palmer J, Makeig S, Kreutz-Delgado K, Rao B (2008) Newton Method for the ICA Mixture Model. Proceedings of the 33rd IEEE International Conference on Acoustics and Signal Processing (ICASSP 2008):1805–1808.

Paus T (2001) Primate anterior cingulate cortex: where motor control, drive and cognition interface. Nat Rev Neurosci 2:417–424.

Piazza C, Miyakoshi M, Akalin-Acar Z, Cantiani C, Reni G, Bianchi AM, Makeig S (2016) An Automated Function for Identifying EEG Independent Components Representing Bilateral Source Activity. In: XIV Mediterranean Conference on Medical and Biological Engineering and Computing 2016 (Kyriacou E, Christofides S, Pattichis CS, eds), pp 105–109 IFMBE Proceedings. Cham: Springer International Publishing.

Pion-Tonachini L, Kreutz-Delgado K, Makeig S (2019) ICLabel: An automated electroencephalographic independent component classifier, dataset, and website. Neuroimage 198:181–197.

Plechawska-Wojcik M, Kaczorowska M, Zapala D (2019) The artifact subspace reconstruction (ASR) for EEG signal correction. A comparative study. In: Information systems architecture and technology: proceedings of 39th international conference on information systems architecture and technology – ISAT 2018: part II (Świątek J, Borzemski L, Wilimowska Z, eds), pp 125–135 Advances in intelligent systems and computing. Cham: Springer International Publishing.

Rousseeuw PJ (1987) Silhouettes: A graphical aid to the interpretation and validation of cluster analysis. Journal of Computational and Applied Mathematics 20:53–65.

Ryvlin P, Picard F (2017) Invasive investigation of insular cortex epilepsy. J Clin Neurophysiol 34:328–332.

Silverman WK, Saavedra LM, Pina AA (2001) Test-retest reliability of anxiety symptoms and diagnoses with the Anxiety Disorders Interview Schedule for DSM-IV: child and parent versions. J Am Acad Child Adolesc Psychiatry 40:937–944.

Sun T, Wang F, Cui J (2015) Insular cortex and insular epilepsy. J Neurol Neurosci 06.

van der Salm SMA, van der Meer JN, Cath DC, Groot PFC, van der Werf YD, Brouwers E, de Wit SJ, Coppens JC, Nederveen AJ, van Rootselaar A-F, Tijssen MAJ (2018) Distinctive tics suppression network in Gilles de la Tourette syndrome

distinguished from suppression of natural urges using multimodal imaging. Neuroimage Clin 20:783–792.

Vogt BA, Pandya DN (1987) Cingulate cortex of the rhesus monkey: II. Cortical afferents. J Comp Neurol 262:271–289.

Weschler D (1999) Wechsler Abbreviated Scale of Intelligence. San Antonio, TX: The Psychological Corporation.

Winkler I, Debener S, Müller K-R, Tangermann M (2015) On the influence of high-pass filtering on ICA-based artifact reduction in EEG-ERP. Conf Proc IEEE Eng Med Biol Soc 2015:4101–4105.

Woods DW, Himle MB (2004) Creating tic suppression: comparing the effects of verbal instruction to differential reinforcement. J Appl Behav Anal 37:417–420.

Supplementary Material

Modulation of frontal oscillatory power during blink suppression in children: Effects of premonitory urge and reward

Makoto Miyakoshi[a*], Joseph Jurgiel[b], Andrea Dillon[b], Susanna Chang[b], John Piacentini[b], Scott Makeig[a], Sandra K. Loo[b]

[a]Swartz Center for Neural Computation, Institute for Neural Computation, University of California San Diego, 9500 Gilman Drive La Jolla CA 92093-0559
[b]Semel Institute for Neuroscience and Human Behavior, University of California, Los Angeles, 760 Westwood Plaza, Los Angeles, CA 90095

*Corresponding author:
Makoto Miyakoshi, Ph.D.
Swartz Center for Neural Computation, Institute for Neural Computation, University of California San Diego
9500 Gilman Drive La Jolla CA 92093-0559 USA
Office Phone: 858-825-7534
Email: mmiyakoshi@ucsd.edu

Contents

1. EEG Preprocessing

We show the step-by-step processes in order below.

1. EEG data were imported from the original recording format to EEGLAB. The digitized channels locations were imported. The scalp channel time-series data were downsampled to 250 Hz.
2. Data were high-pass filtered with cutoff frequency at 1.5 Hz (FIR, Blackman window, transition bandwidth 1.0Hz, filter order 1376) and low-pass filtered at 55 Hz (FIR, Blackman window, transition bandwidth 10Hz, filter order 138). The relatively high cutoff frequency for high-pass filter is to enforce stationarity of the data to facilitate ICA (Winkler et al. 2015). The low-pass filter is to suppress the line noise at 60 Hz.
3. clean_rawdata() plugin including ASR was applied with the following parameters: channel rejection for poor correlation with surrounding channels, 0.75; ASR with correction criterion in SD, 8; and the final window rejection for poor data quality, 0.5. See Supplementary Material 5 for detail of the algorithm used in ASR.
4. Spline interpolation was applied to the rejected channels. This is to compute an unbiased average-reference potential in the next step.
5. Average reference was applied to the data. In doing so, the original reference channel, which is continuous zeros, was included so that the averaging did not change data rank.
6. Single-model adaptive mixture ICA (AMICA) (Palmer et al. 2008, 2016; Delorme et al. 2012; Hsu et al. 2018) was performed decomposition with the following

parameters: SD for datapoint rejection, 3; number of rejection, 15. This set of parameter rejects around 10% of data points only for the AMICA purpose.

7. Equivalent current dipoles were fit using Fieldtrip (Oostenveld et al. 2011) for scalp projections of the independent components. Symmetric two dipoles were fitted where necessary (Piazza et al. 2016).
8. EEGLAB plugin ICLabel() was used to generate probabilistic labels such as ‘Brain’, ‘Eye’, ‘Muscle’ for each IC (Pion-Tonachini et al. 2019) to evaluate impact of ICA-decomposed eye component source activations on scalp sensor signals.
9. Independent component selection was performed in the following way. Using EEGLAB STUDY, all subjects’ ICs whose equivalent dipole locations were inside the MNI brain mask and have less than 15% residual variance (i.e., comparison between the ideal dipolar projection on the scalp and the empirically obtained scalp topography of ICs) were classified into 30 clusters using k-means algorithm on IC’s precomputed power spectral density (PSD). Clusters with non-brain PSDs were selected for rejection. By backprojecting the remaining IC clusters, individual data were reconstructed. All of these processed were performed using EEGLAB plugin *std_clust2ch()*.
10. Using the reconstructed data, individual data were processed for the final group-level clustering analysis. First, the continuous data were epoched into +/- 5.7 s windows relative to blink ERP peak. The epochs were labeled for ‘No Supp’ ‘Supp’ ‘Supp Rwd’ according to the block-separated conditions they belong to. Then, EEGLAB STUDY was built again for the final statistics. For each subject and condition, event-related spectral perturbation (ERSP) (Makeig 1993) was computed using the following parameters: Frequency range, 1 to 55 Hz, number of wavelet cycles, from 3 to 15 (linear increase), sliding window width, 3340 ms, number of output times, 403 (so that the mean window step size is about 20 ms starting from -4030 to 4026 ms), number of frequency bins, 100. Baseline period was defined from -4000 to -3000 ms (see Supplementary Material 3 for the rationale for this decision). K-means clustering was performed using IC dipole locations only without any time-frequency data to avoid circular inference in the subsequent statistical tests (Kriegeskorte et al. 2009). The number of clusters was determined by using optimization algorithms including Silhouette (Rousseeuw 1987), Davies-Bouldin (Davies and Bouldin 1979), and Calinski-Harabasz (Calinski and Harabasz 1974) to see if their suggestion would converge.

We adopted the minimum number suggested to maximize the unique subject ratio per IC cluster.

2. Influence of Eye-IC on Scalp Sensor Data

To evaluate the influence of blink artifact on scalp sensor data, we examined group-level ERPs that were averaged across the eight front most channels located around the forehead (see Figure S1). The ERPs were time-locked to single-trial EOG peak latency. We compared the ERPs across the following three conditions: 1) minimally cleaned sensor data (only outliers were removed); 2) re-constructed scalp sensor data by back-projecting 180/4464 ICs (from all 35 participants) labeled as 'Eye' with > 0.50 probability, 3) re-constructed scalp sensor data by back-projecting 910/3224 ICs (from the finally selected 26 participants) that were qualified brain components submitted for the final group-level analysis. The results showed that the back-projection of 180 eye ICs modeled the high-amplitude EOG almost completely (Figure S1). This indicated that ICA successfully captured nearly the entire variance of EOG artifact with as little as 4% of the total number of ICs, and the remaining ICs are maximally independent (i.e. free of) this ocular artifact. To demonstrate the scale difference between the backprojections of decomposed EOG components and the finally selected qualified brain components, ERP of the latter was overlaid on Figure S1.

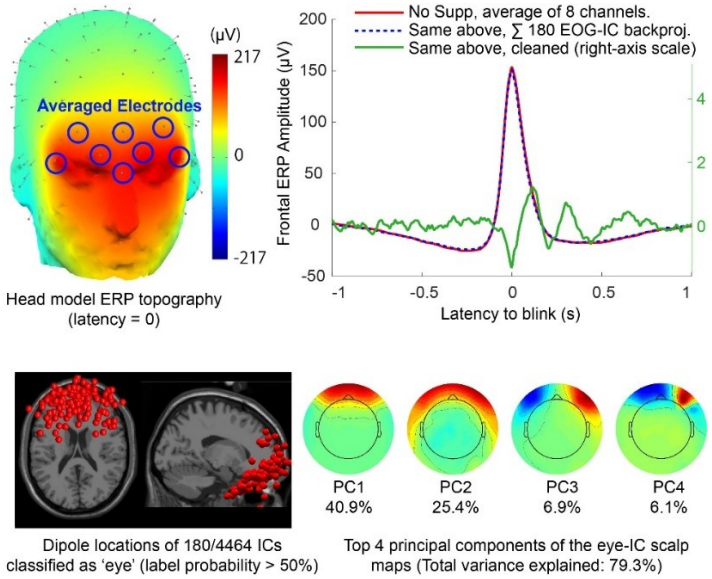

Figure S1. Top left, the head topography of blink ERP at the peak latency. The front most scalp electrode locations were shown. The ERPs recorded at these electrodes were averaged to serve as representative blink ERP. Top right, the comparison across

minimally processed raw blink ERP, the scalp back projection of 180/4464 'eye' independent components (ICs) identified by ICLabel algorithm (Pion-Tonachini et al. 2019) with label probability > 50%, and the scalp back projection of 910/3224 qualified brain ICs used for the final analysis. Note the difference in the two amplitude scales shown in the left and the right vertical axes. Bottom left, the equivalent current dipole locations of the 'eye' ICs. Bottom right, mean scalp topographies of top 4 principal components (PCs) obtained from the scalp topographies of 'eye' ICs. PC1 and PC2 correspond to blink and/or vertical eye movement, while PC3 and PC4 horizontal eye movement.

3. Main effect of Suppression and Urge on EOG

Next, we tested whether blink behavior, characterized by ERPs time-locked to the EOG peak, was affected by Suppression and/or Urge. The ERPs of the minimally cleaned data averaged across the eight forehead sensors tested in Figure S1 were compared. The results did not show statistical differences across Suppression conditions (Figure S2). However, when trials were separated into High and Low Urge conditions, the difference between the two EOG peak amplitudes reached significance when uncorrected for multiple comparisons. Although the uncorrected statistical result requires caution for interpretation, the smaller EOG peak for Urge Low may indicate that when subjective urge is low (or unmonitorable), the corresponding blink may be physically smaller than High Urge blinks.

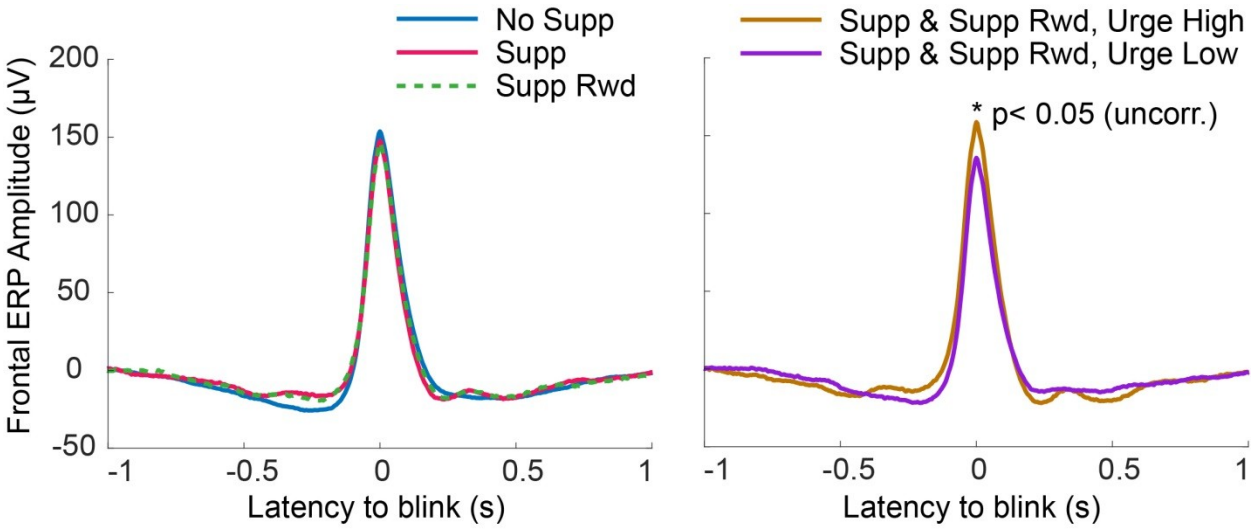

Figure S2. Blink ERPs separated into experimental conditions. Left, the condition Suppression was tested. The peak ERP amplitude did not show statistical difference.

Right, the condition Urge was tested. The peak ERP amplitude showed statistical difference at an uncorrected p-value.

Scalp-ERP Comparison Between Before and After Data Cleaning

To study the effect of artifact removal, we compared scalp sensor-level 128 ch ERPs before and after the data cleaning processes (Figure S3). It is clear that the blink ERP has high amplitude and broad distribution along with the anterior-posterior axis of the head. It is notable that after artifact rejection, the amplitude scale was nearly 25 times reduced. Also, the anterior-posterior distribution of the ERP did not show a classical, well-defined waveform. The visual impression motivated us to use time-frequency decomposition as the main analysis approach rather than quantifying ERP waveforms.

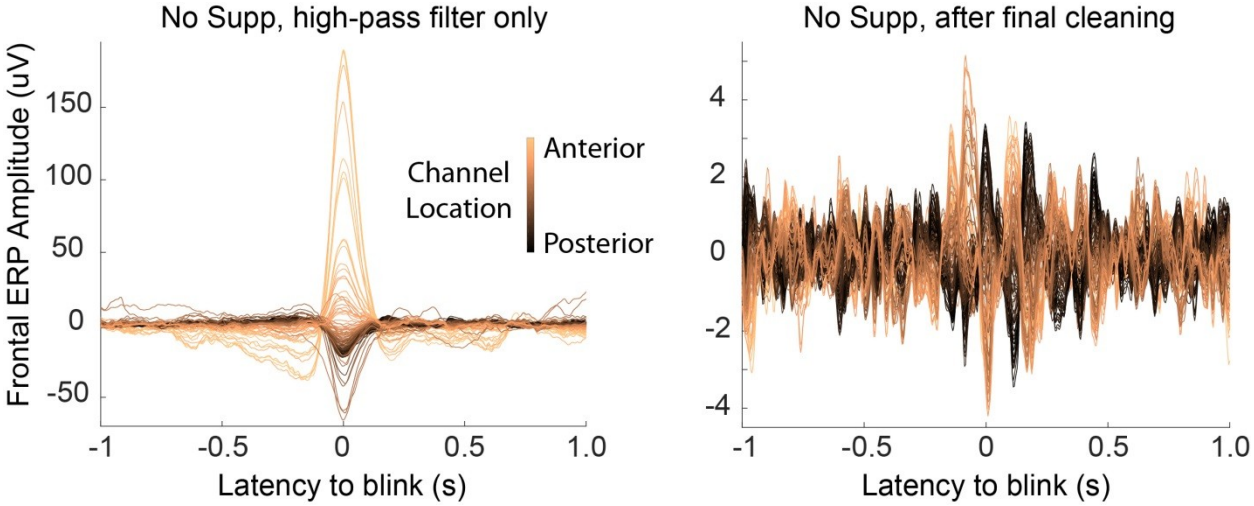

Figure S3. The grand-mean ERP butterfly plots of 128 scalp sensor recordings. The plotting color scale represents y axis coordinates of the electrodes on the template MNI head. Left, minimally processed ERP data. Right, after final cleaning. Note the amplitude scale difference between the two plots (200 μV vs. 8 μV). One may be concerned about the drastic amplitude reduction and wonder if targeted brain signals still remain. This question is answered in Extended Data 4 by a post-hoc validation test.

4. Histogram of blink occurrence.

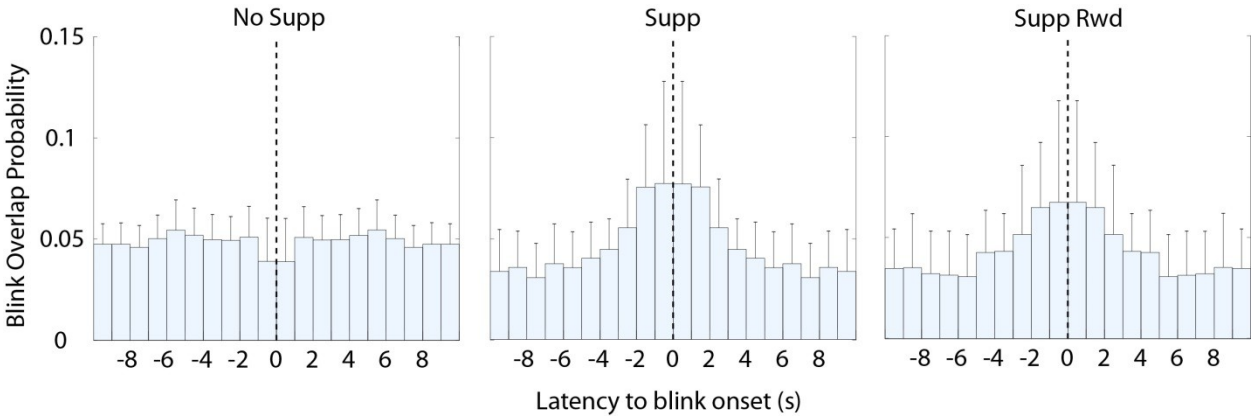

Figure S4. Histogram of blink probability relative to a blink ERP peak. The rise toward latency zero started at around -3 s. Based on this evaluation, we determined to set the baseline period in our event-related spectral perturbation to be -4 to -3 s.

5. Post-hoc Validation of EEG Preprocessing

In the previous section, we reported that mean of 99.7% of variance was reduced from the raw data. This number may appear surprisingly large if one is not familiar with these data cleaning statistics, and may wonder if EEG signal is still present after the cleaning. This is a legitimate and critical question that concerns validity of data presented here.

To answer this question properly, ideally we would need a study with a known signal embedded as ground truth to calculate change of signal-to-noise ratio (SNR) between before and after the cleaning process. However, such a ground truth signal is usually unavailable for a standard human EEG study. The present study does not include such a design for hard validation either. We cannot obtain analytic solution to determine the effect of data cleaning process either, since results from ASR and ICA are data dependent. However, it seems still possible to perform a post-hoc validation to provide, at least, some type of lower bound of confidence interval of the current cleaning method and insight for quantitative characteristics relevant to it. This validation, however, critically depends on assumptions of ICA and how it works. The schematic illustration for the procedure of the post-hoc validation is shown in Figure S5.

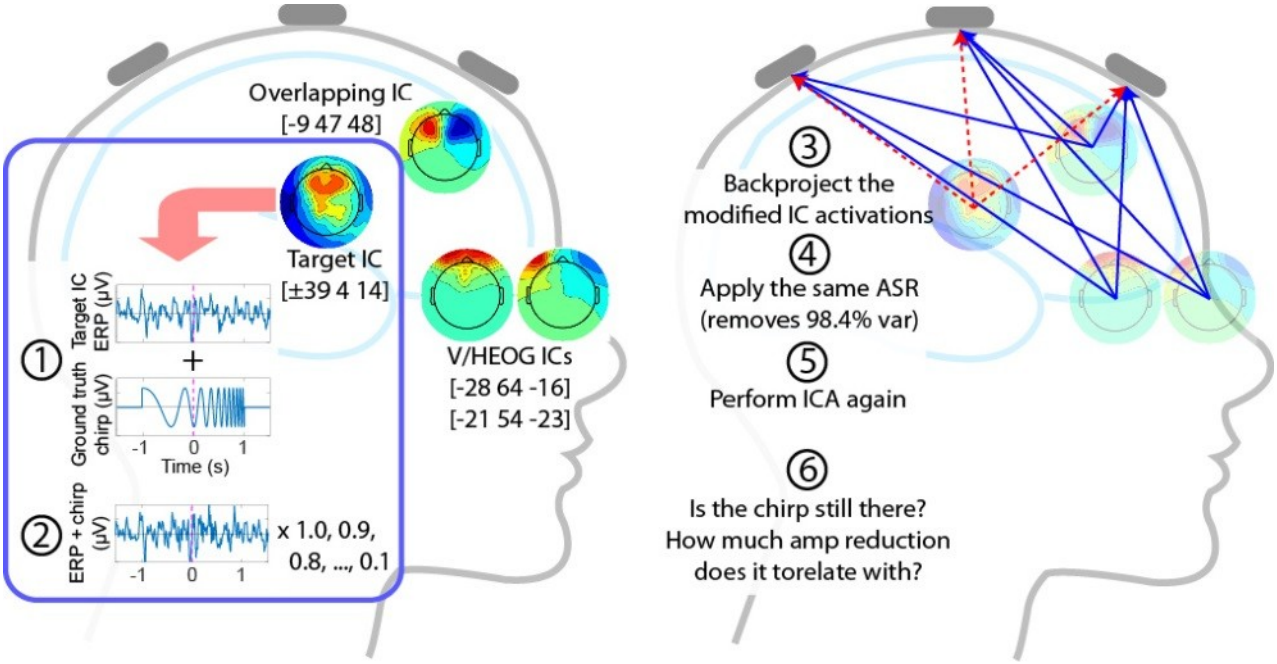

Figure S5. Schematic illustration of the procedure used in the post-hoc validation.

Below, we describe the procedure step by step.

1. A single subject from whom we obtained the least number of the ICs (10) for the final analysis was chosen for this validation. This is to assume the worst case scenario where data were most challenged in terms of quality of ICA results among all the subjects. We gave additional and more aggressive data cleaning based on manual data-window rejection on this dataset only for the purpose of the current post-hoc validation study and ran the second ICA so that the definition of 'clean EEG' and the associated ICA weight matrix is best maintained. From the second ICA, we obtained 14 ICs classified as 'brain' with > 0.8 probability by *IClabel()* plugin (Pion-Tonachini et al., 2019). We copied this ICA weight matrix to the same subject's raw EEG data (after rejecting the same channels rejected for the ICA 116 ch, the same referencing to average, and applying the same high-pass filter). Thus, the raw scalp EEG data were decomposed with ICA calculated from the aggressively cleaned data, though the artifacts rejected by ASR were still fully present. We selected one of the 'brain'-labeled ICs (probability: 0.90) that was localized in the frontal lobe whose Talailach coordinate [+/-39 4 14]; symmetrically bilateral dipoles were fit suggested by *twoDipoleFit()* plugin (Piazza et al. 2016). Henceforth this IC will be referred to as *target IC*. Also, in order to evaluate potential leakage from the

target IC due to crosstalk between ICs by imperfectly achieved temporal independence, we selected another IC localized at [-7 59 36] whose scalp projection showed overlap with that of *target IC*. Henceforth, this IC will be referred to as *overlapping IC*. Finally, we selected vertical EOG/blink and horizontal EOG ICs as *eye ICs* (label probability: 0.86 and 0.99). We calculated variance of the *target IC* and the *eye ICs* between -1 to 1 s relative to blink ERP peak to calculate signal-to-noise ratio (SNR), which is defined as 20*log10(var(*target IC*)/var(*eye ICs*)) in terms of representative ocular artifacts. The SNR for the horizontal and vertical/blink *eye ICs* were averaged into a single value.

2. A chirp signal (log-scale increase from 10 to 50 Hz, -1 to 1 s relative to blink ERP peak) was added to the single-trial ERP of *target IC.* This chirp signal was scaled to have only 1% of standard deviation of the corresponding raw signal (7.05 vs. 0.07) so that it impacts performance of ICA minimally (see quantitative comparison below). This low-amplitude short-burst chirp signal served as a ground truth, representing a pre-defined time-frequency characteristics that is time-locked to blink ERP peak. Care was taken not to affect the statistical characteristics of the time-series data of the *target IC*: The comparison before and after adding the chirp signal showed that standard deviation was 7.0461 vs. 7.0466 (0.07% change), skewness was -1.7569 vs. -1.7564 (0.03% change), and kurtosis was 52.4106 vs. 52.3946 (0.03% change), respectively. Overall, the effect of adding the chirp to the original signal was < 0.1%, which was expected to have only negligible influence in the subsequent ICA.
3. The IC activation time series, including the embedded chirp signal in the *target IC* activations, was backprojected to scalp sensors. In this way, the scalp sensor data were reconstructed with the ground truth signal during the peri-blink period. Importantly, this backprojection was performed 10 times while the amplitude of the *target IC* activations was reduced from 100% to 10% with 10% step. Henceforth, the backprojected (BP) data with reduced *target IC* amplitude will be referred to as $BP_{targetIC\_100\%}$, $BP_{targetIC\_90\%}$, $BP_{targetIC\_80\%}$, $BP_{targetIC\_70\%}$, ..., $BP_{targetIC\_10\%,}$ and the original unmodified ICA result as $BP_{original}$.
4. The backprojected scalp channel data were processed with the ASR with the same parameters used in the main study.
5. ICA was performed with the same parameters used in the main study.

6. The decomposed ground truth signal after various levels of SNR reduction was evaluated to determine how much SNR loss can be tolerated by the current cleaning method (ASR + ICA), thus to estimate the lower bound of confidence interval and margin for the current data in the worst case scenario.

The results are plotted Table S1 and Figure S6. Before and after ASR, SNR gain of 3.89 dB was confirmed. As the amplitude scale of the *target IC* was reduced progressively, the SNR decreased in relatively linearly. However, IC scalp topography correlation coefficient showed a clear knee point at amplitude scaling to 40%, which was determined by finding a bisection point that minimizes the sum of errors for the two linear line fits. The SNR difference between 100% and 40% amplitude scaling points was 0.63 - (-6.34) = 6.97 dB. This amount of SNR may be interpreted as a margin from the lower bound of confidence interval of the analysis used in the current study.

Table S1. The target IC statistics for $BP_{original}$, $BP_{targetIC\_100\%}$ to $BP_{targetIC\_10\%}$.

	Orig.	100 %	90%	80%	70%	60%	50%	40%	30%	20%	10%
Target IC variance	4.560	4.656	3.811	3.149	2.456	1.964	1.499	0.978	0.693	0.517	0.241
Variance rank	3	3	5	6	8	8	11	16	19	21	40
Scalp topo corr.	1.000	0.995	0.999	0.991	0.973	0.967	0.938	0.934	0.876	0.741	0.639

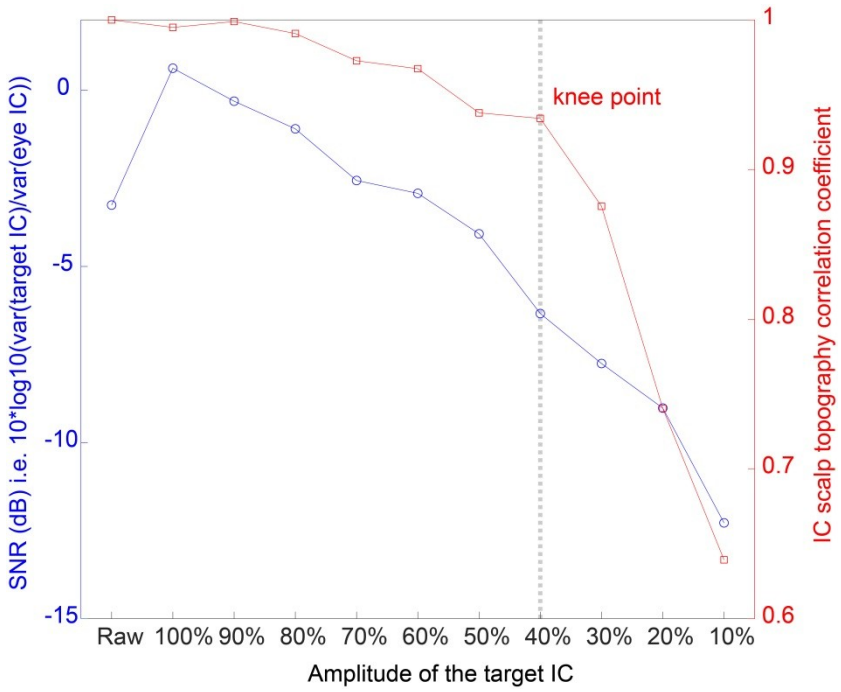

Figure S6. Changes of SNR, defined by target IC variance over eye IC variance, and IC scalp topography correlation with the original ICA decomposition along with amplitude scale reduction of the target IC. The knee point defined by bisection point by two line fitting that minimizes error was found at 40%, suggesting that the ASR+ICA method used in the current study has margin of 6.97 dB in SNR.

Next, we evaluated how the implemented ground truth survived the ASR + ICA cleaning processes. The results are shown in Figure S7. The target IC did not show visually identifiable modulation in ERSP. However, inter-trial phase coherence (ITC) showed the time-frequency signature of the ground-truth chirp signal surprisingly robustly down to the scale reduction to 10% (SNR loss of 12.90 dB). The result indicates that the current ASR+ICA approach can detect weak signal robustly (as long as they fit the assumption of ICA) and does not critically affect time-frequency characteristics.

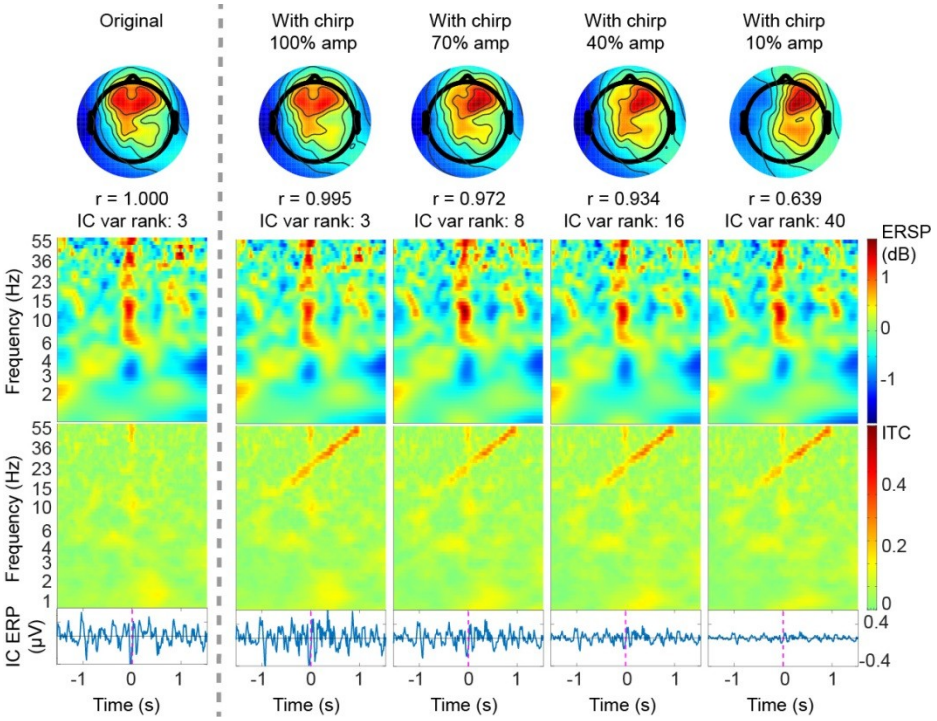

Figure S7. Time-frequency analysis on the target IC during peri-blink period. Event-related spectral perturbation (ERSP, the second row) did not show the signature of chirp, but inter-trial phase coherence (ITC, the third row) detected the chirp pattern down to 10% amplitude scale. ERSP was calculated as a power ratio against mean power value during the baseline period, hence it remained unaffected by the general amplitude reduction. The IC ERP waveforms (the bottom row) showed progressively diminishing amplitude. The result demonstrated that the small-amplitude (1% variance of the component) ground truth signal survived ASR+ICA data cleaning method used in this study even when the component amplitude was reduced to 10 % (SNR loss of 12.90 dB).

Finally, we evaluated potential leak or crosstalk effect due to insufficient decomposition between *target IC* and *overlapping IC* as the amplitude scale for the *target IC* was reduced. This test may be understood as testing specificity, in contrast with sensitivity shown in Figure S8. Since we confirmed ERSP did not show noticeable evidence of the presence of the ground-truth chirp signal, we focused only on ITC differences from the original ITC results. The results are shown in Table S2 and Figure S8. The characteristic time-frequency pattern of the chirp became noticeable as the amplitude downscaling on the *target IC* progressed, indicating potential leak or

crosstalk between ICs was confirmed. Note that 70% condition also showed noticeable chirp (data not shown), indicating the leak/crosstalk effect is nonlinear.

Table S2. The overlapping IC statistics for $BP_{original}$, $BP_{targetIC\_100\%}$ to $BP_{targetIC\_10\%}$

	Orig.	100 %	90%	80%	70%	60%	50%	40%	30%	20%	10%
Overlap. IC var.	1.478	1.515	1.527	1.461	1.534	1.516	1.513	1.420	1.479	1.458	1.508
Variance rank	12	12	12	12	12	12	12	11	11	11	11
Scalp topo corr.	1.000	0.999	0.999	0.987	0.908	0.986	0.987	0.983	0.972	0.965	0.983

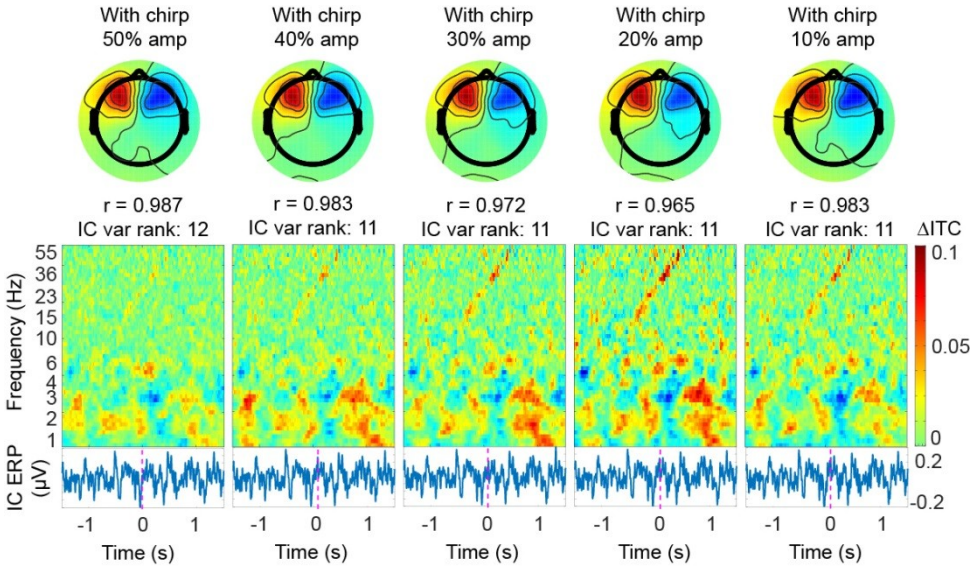

Figure S8. Time-frequency analysis on the overlapping IC during peri-blink period. ITC differences (i.e., subtractions) from the original data ITC are shown. Because target IC and overlapping IC are by definition temporally maximally independent, the characteristic time-frequency pattern of the ground-truth chirp signal should not be present in the overlapping IC. However, due to the progressive SNR reduction by reducing the target IC amplitude, ICA started to fail to keep the ground truth signal only to the target IC. This may be understood as leakage or crosstalk between ICs under progressively challenging situation in terms of SNR. Note the difference of color scale used in Figure S7 (0.6 vs. 0.1) which indicates minor magnitude of this phenomenon.

In summary, we attempted to answer to the legitimate skepticism that such a heavy artifact rejection preprocess that removes more than 99% of data variance may also lose signal of interest altogether. The results from the post-hoc validation tests confirmed that 1) ASR alone showed 3.89 dB of SNR gain; 2) deterioration of IC scalp projection was observed when signal variance was reduced to less than 40%; 3) Time-frequency characteristics of the ground truth signal survived ASR + ICA processes even with 12.90 dB of SNR loss (evaluation of sensitivity); 4) Inter-IC leakages or cross-talk started to happen when signal variance was reduced to less than 40% (evaluation of independence). We concluded that target single can tolerate with variance reduction down to 40%, which is SNR reduction of 6.97 dB. This value indicates SNR margin in this example scenario, which can be understood as lower bound of confidence interval of the entire processing methods we used in the current study. Among similar studies, such validation is rarely shown. We hope our attempt here showed the level of reliability we expect to our data, and demonstrated an idea of performing quantitative evaluation of ASR-ICA approach, which can be further extended to be a separate methodological development by taking advantage of data decomposition using ICA.

6. Description of Artifact Subspace Reconstruction (ASR)

In the conventional scalp EEG studies, it was a widely believed that that EEG recording during blink must be rejected (Picton et al. 2000). A common practice to perform this is to use an amplitude threshold for a rejection criterion, and representative value could be anywhere between +/-75 and 200 μV. However, our question was to investigate brain dynamics related to blink. To analyze such data, we used two artifact rejection approaches, namely artifact subspace reconstruction (ASR) and independent component analysis (ICA) to address the issue of stationary and non-stationary artifact, respectively. A historical fact is that the offline version of artifact subspace reconstruction (ASR) implemented in *clean_rawdata()* plugin, which is now validated by multiple studies (Mullen et al. 2015; Chang et al. 2018, 2019; Gabard-Durnam et al. 2018; Blum et al. 2019; Plechawska-Wojcik et al. 2019), was specifically developed for this project upon our request by the main developer of BCILAB (Kothe and Makeig 2013). The original solution was called *Christian-Nima Combo* after the developers, but formally changed into *clean_rawdata()* on June 26, 2013 to be implemented as an plugin for EEGLAB (Delorme and Makeig 2004). The detail of the algorithm is described below.

Importantly, ASR works in a complementary way with ICA; ASR uses sliding-window interpolation (to be exact, subspace reconstruction using principal component analysis) to correct non-stationary artifacts that ICA cannot handle. This solution improves data stationarity, which is a critical assumption for ICA that practically works as a requirement to obtain good performance.

Artifact subspace reconstruction (ASR) removes short-duration, high-amplitude artifacts in the continuous data using 0.5-s sliding window with 50% overlap and linear blending. The detailed flow of the process is explained here. Let $X_{calibrate} \in \Re^{Q \times M}$ be 'the cleanest part of the channel data' which ASR finds for calibration for Q-channel continuous EEG data. This is achieved by first applying infinite impulse response (IIR) spectral weighting (8th order Yule-Walker) that is the inverse of an in-house developed heuristic model of EEG power spectral density that has 1/f curve with an attenuated lower-frequency end and a peak at around 8 Hz, then concatenating windows of time-series by z-scored RMS amplitude of the time series between -3.5 and 5.5 after. Let $\bar{M}$ the square root of the covariance matrix C of $X_{calibrate}$ such that $\bar{M}\bar{M}^T = Cov[X_{calibrate}]$ where $\bar{M}^T$ represents transpose of $\bar{M}$. Let $x_{(t)} \in \Re^Q$ be a EEG sample at time point t, and let $X \in \Re^{Q \times N}$ be the sliding window of data containing $x_{(t)}$. Principal component (PC) analysis (PCA) is applied to X to obtain PCs of the currently selected window $V = [v_1 \ldots v_Q] \in \Re^{Q \times Q}$. Those PCs V whose variance d_k exceeds an omnibus cutoff threshold $h(v_k)$ are determined as *artifact subspace*. The omnibus cutoff threshold h_k is defined as follows. Let $M = V^T \bar{M}$ be projection of $\bar{M}$ into PC space. Principal component analysis on $X_{calibrate}$ is computed to obtain $W = [w_1 \ldots w_Q] \in \Re^{QxQ}$ and activations $Y = W^T X_{calibrate}$. For activation of each component Y_k, root-mean-square amplitude is calculated to obtain robust mean $\mu_{calibrate}$ and standard deviation $\sigma_{calibrate}$. The omnibus threshold is

obtained as $h_k = \mu_{calibrate_k} + \sigma_{calibrate_k} \times f_{user}$ where f_{user} represents user-specified factor for SD. For the current analysis, we chose $f_{user} = 8$ which is a very lax criterion, intending only to remove large outlier activations in the time-series data in order to let the subsequent ICA decompose artifacts that have physiological sources, such as eye blinks/movements, EMG, and ECG.

After artifact subspace is determined, the threshold operator $U \in \Re^{Q \times Q}$ is built. For this, the omnibus threshold h_k in the channel space needs to be projected to the PC space $h(v_j)$ as $h(v_j) = \sum_k \left[(\mu_{calibrate_k} + \sigma_{calibrate_k} \times f_{user}) W_k^T V_j \right]^2$ to be compared with d_j. Now, U_{jl} is built such that $U_{jl} = 0$ if $d_j > h(v_j)$ to remove them, otherwise $U_{jl} = 1$ to keep them. After removing artifact subspace, it is interpolated, which completes the process *artifact subspace reconstruction.* This process is represented by the linear operator $R = VM(M \circ U)^+ V^T$ such that $\hat{x}_{(t)} = Rx_{(t)}$ produces corrected data $\hat{x}_{(t)}$ for input data $x_{(t)}$. $M \circ U$ represents element-wise multiplication of M and U, and $(M \circ U)^+$ represents Moore-Penrose pseudoinverse of $(M \circ U)$.

7. ERSP results for all clusters, all conditions.

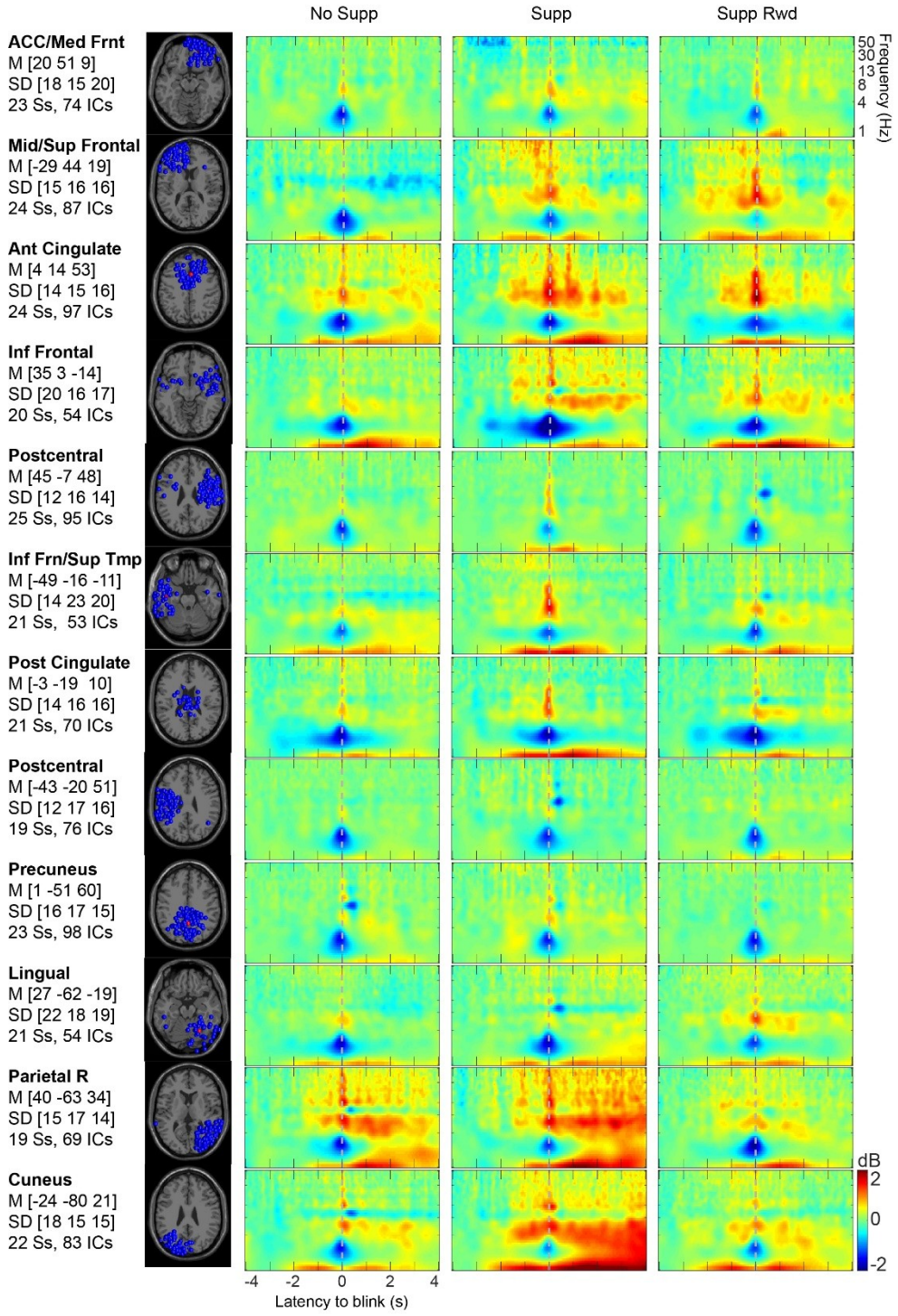

Figure S9. Event-related spectral perturbation (ERPS) plots showing grand-mean power (across independent components) for each condition (No Supp, Supp, Supp Rwd). The color plotting scheme is in dB, indicating that each pixel power value is converted into

ratio by dividing mean power during the baseline period (-4 to -3 s) within the same frequency bin.

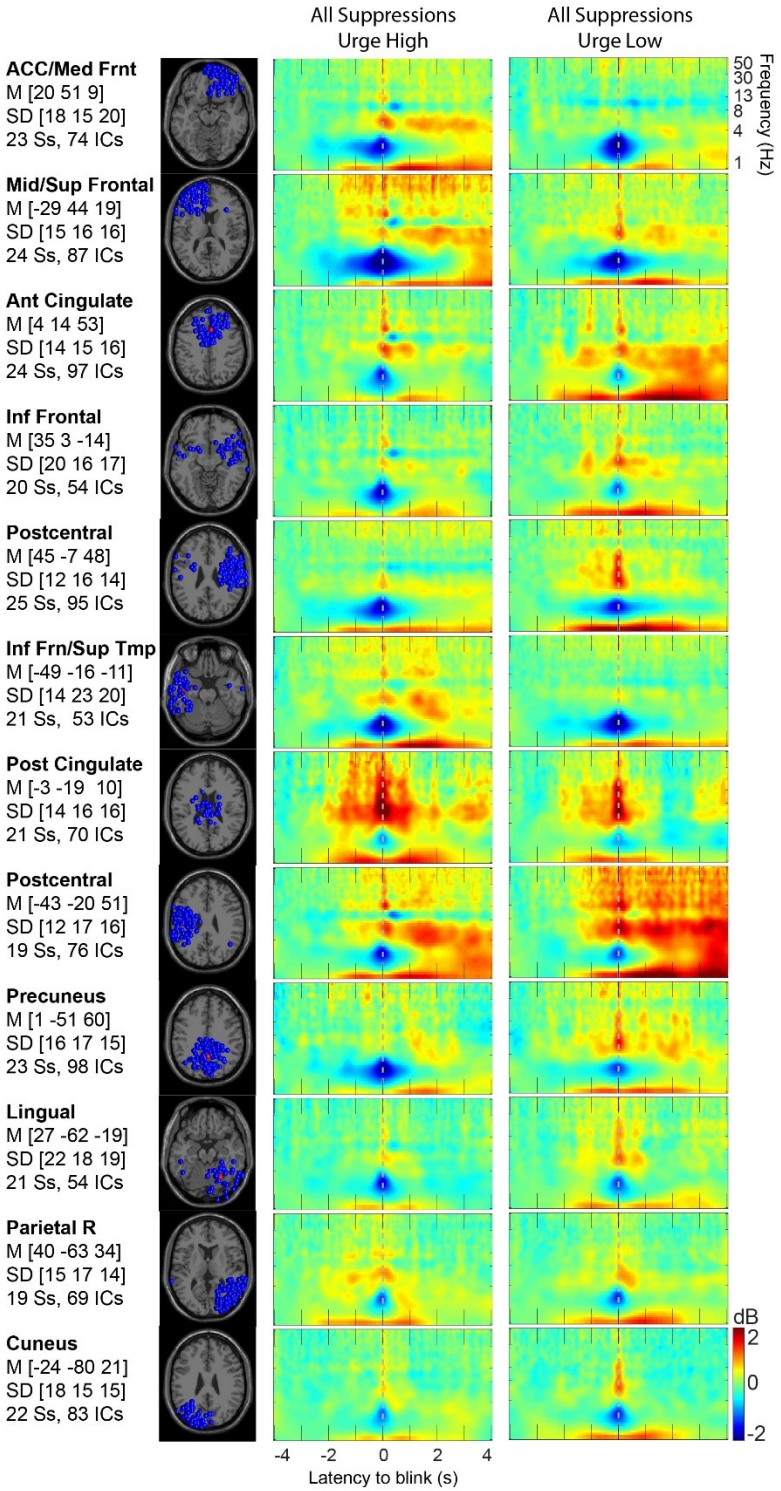

Figure S10. Event-related spectral perturbation (ERPS) plots showing grand-mean power (across independent components) for each condition (Urge High, Urge Low). The color

plotting scheme is in dB, indicating that each pixel power value is converted into ratio by dividing mean power during the baseline period (-4 to -3 s) within the same frequency bin.

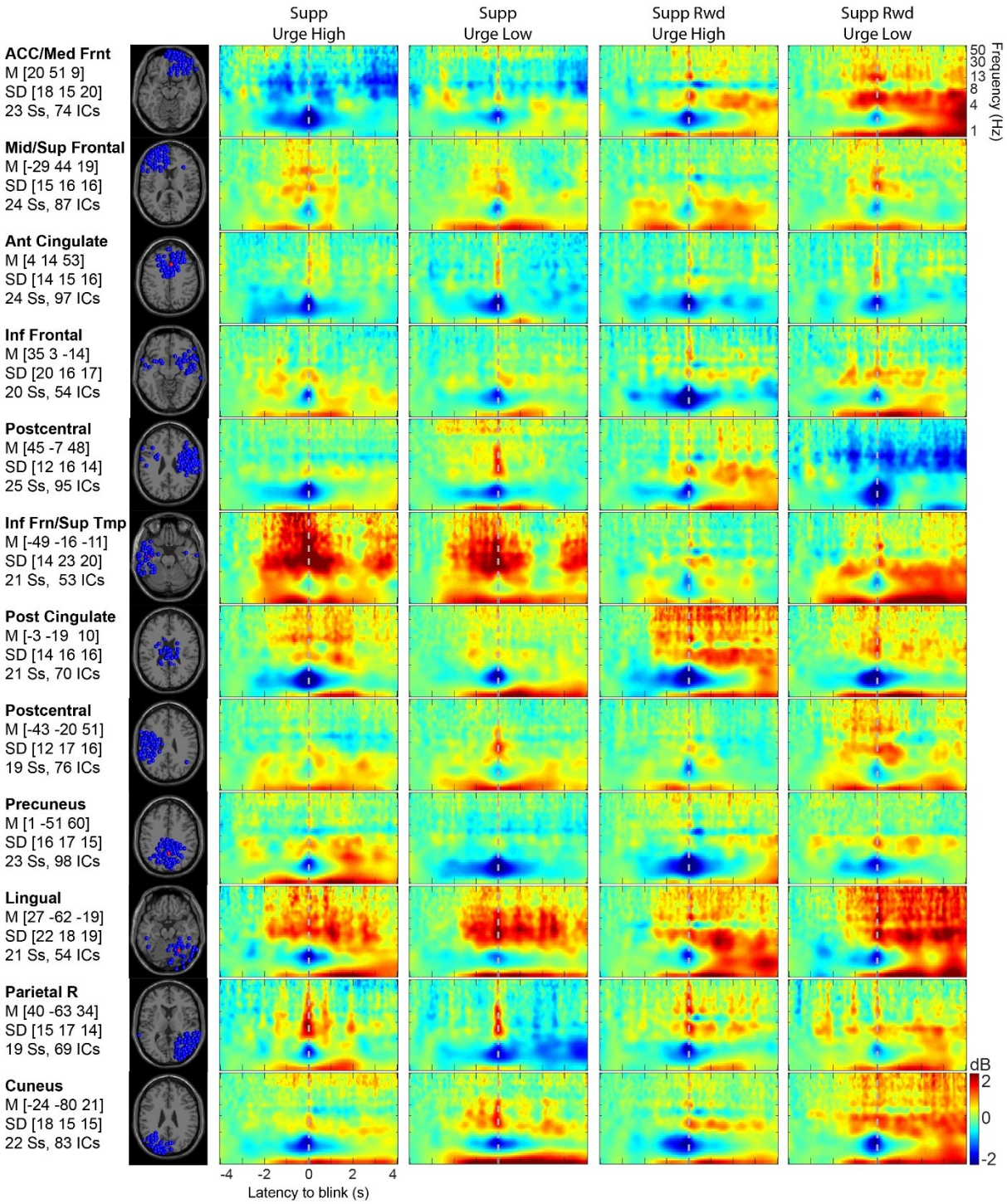

Figure S11. Event-related spectral perturbation (ERPS) plots showing grand-mean power (across independent components) for each of 2 x 2 combination of conditions (Supp-Supp Rwd vs. Urge High-Urge Low). The color plotting scheme is in dB, indicating that each pixel power value is converted into ratio by dividing mean power during the baseline period (-4 to -3 s) within the same frequency bin.

8. Bibliography

Blum S, Jacobsen NSJ, Bleichner MG, Debener S. 2019. A riemannian modification of artifact subspace reconstruction for EEG artifact handling. Front Hum Neurosci. 13:141.

Calinski T, Harabasz J. 1974. A dendrite method for cluster analysis. Communications in Statistics - Theory and Methods. 3:1–27.

Chang C-Y, Hsu S-H, Pion-Tonachini L, Jung T-P. 2018. Evaluation of artifact subspace reconstruction for automatic EEG artifact removal. Conf Proc IEEE Eng Med Biol Soc. 2018:1242–1245.

Chang C-Y, Hsu S-H, Pion-Tonachini L, Jung T-P. 2019. Evaluation of Artifact Subspace Reconstruction for Automatic Artifact Components Removal in Multi-channel EEG Recordings. IEEE Trans Biomed Eng.

Davies DL, Bouldin DW. 1979. A Cluster Separation Measure. IEEE Trans Pattern Anal Mach Intell. PAMI-1:224–227.

Delorme A, Makeig S. 2004. EEGLAB: an open source toolbox for analysis of single-trial EEG dynamics including independent component analysis. J Neurosci Methods. 134:9–21.

Delorme A, Palmer J, Onton J, Oostenveld R, Makeig S. 2012. Independent EEG sources are dipolar. PLoS One. 7:e30135.

Gabard-Durnam LJ, Mendez Leal AS, Wilkinson CL, Levin AR. 2018. The Harvard Automated Processing Pipeline for Electroencephalography (HAPPE): Standardized Processing Software for Developmental and High-Artifact Data. Front Neurosci. 12:97.

Hsu S-H, Pion-Tonachini L, Palmer J, Miyakoshi M, Makeig S, Jung T-P. 2018. Modeling brain dynamic state changes with adaptive mixture independent component analysis. Neuroimage. 183:47–61.

Kothe CA, Makeig S. 2013. BCILAB: a platform for brain-computer interface development. J Neural Eng. 10:056014.

Kriegeskorte N, Simmons WK, Bellgowan PSF, Baker CI. 2009. Circular analysis in systems neuroscience: the dangers of double dipping. Nat Neurosci. 12:535–540.

Makeig S. 1993. Auditory event-related dynamics of the EEG spectrum and effects of exposure to tones. Electroencephalogr Clin Neurophysiol. 86:283–293.

Mullen TR, Kothe CAE, Chi YM, Ojeda A, Kerth T, Makeig S, Jung T-P, Cauwenberghs G. 2015. Real-Time Neuroimaging and Cognitive Monitoring Using Wearable Dry EEG. IEEE Trans Biomed Eng. 62:2553–2567.

Oostenveld R, Fries P, Maris E, Schoffelen J-M. 2011. FieldTrip: Open source software for advanced analysis of MEG, EEG, and invasive electrophysiological data. Comput Intell Neurosci. 2011:156869.

Palmer J, Kreutz-delgado K, Makeig S. 2016. AMICA: An Adaptive Mixture of Independent Component Analyzers with Shared Components.

Palmer J, Makeig S, Kreutz-Delgado K, Rao B. 2008. Newton Method for the ICA Mixture Model. Proceedings of the 33rd IEEE International Conference on Acoustics and Signal Processing (ICASSP 2008). 1805–1808.

Piazza C, Miyakoshi M, Akalin-Acar Z, Cantiani C, Reni G, Bianchi AM, Makeig S. 2016. An Automated Function for Identifying EEG Independent Components Representing Bilateral Source Activity. In: Kyriacou E, Christofides S, Pattichis CS, editors. XIV Mediterranean Conference on Medical and Biological Engineering and Computing 2016. IFMBE Proceedings. Cham: Springer International Publishing. p. 105–109.

Picton TW, Bentin S, Berg P, Donchin E, Hillyard SA, Johnson R, Miller GA, Ritter W, Ruchkin DS, Rugg MD, Taylor MJ. 2000. Guidelines for using human event-related potentials to study cognition: recording standards and publication criteria. Psychophysiology. 37:127–152.

Pion-Tonachini L, Kreutz-Delgado K, Makeig S. 2019. ICLabel: An automated electroencephalographic independent component classifier, dataset, and website. Neuroimage. 198:181–197.

Plechawska-Wojcik M, Kaczorowska M, Zapala D. 2019. The artifact subspace reconstruction (ASR) for EEG signal correction. A comparative study. In: Świątek J, Borzemski L, Wilimowska Z, editors. Information systems architecture and technology: proceedings of 39th international conference on information systems architecture and technology – ISAT 2018: part II. Advances in intelligent systems and computing. Cham: Springer International Publishing. p. 125–135.

Rousseeuw PJ. 1987. Silhouettes: A graphical aid to the interpretation and validation of cluster analysis. Journal of Computational and Applied Mathematics. 20:53–65.

Winkler I, Debener S, Müller K-R, Tangermann M. 2015. On the influence of high-pass filtering on ICA-based artifact reduction in EEG-ERP. Conf Proc IEEE Eng Med Biol Soc. 2015:4101–4105.